Theoretical Notes

Note 316

12 January 1981

Electrical Breakdown Characteristics of Soil Samples

C. Mallon, R. Denson, R. E. Leadon, and T. M. Flanagan

JAYCOR
San Diego, California 92138

TABLE OF CONTENTS

LIST OF ILLUSTRATIONS

LIST OF ILLUSTRATIONS (Continued)

ABSTRACT

The electrical breakdown characteristics of small cylindrical samples of soil subjected to voltage pulses have been measured. The threshold electrical field for breakdowns to occur, the breakdown delay time as a function of the applied electric field, and the sample I-V characteristics during the breakdowns are presented. Evidence is cited which indicates that the breakdown process is due to ionization of the air in the voids between the soil grains. A semiempirical equivalent-circuit model is presented and fitted to the sample I-V characteristics during breakdown.

SECTION I

INTRODUCTION

In a previous note (ref. 1), the low-field electrical characteristics of soil samples obtained from the Siege Development Facility (SDF) in Albuquerque, New Mexico were presented. The data presented is applicable in the linear response regime for relatively small magnitudes of the applied electrical fields. However, they are not adequate to describe the electrical responses of the soil when the applied fields are large enough to cause the soil to break down electrically.

The breakdown characteristics of dielectrics are usually characterized by a threshold electrical field (E_{BD}) below which the dielectric never breaks down, and a curve of the delay time versus electric field ($E > E_{BD}$) for the onset of the breakdown after the application of E. In addition, for soils, the I-V characteristics during the breakdown are of interest.

In the present note, experimental data are presented for the threshold field, delay times, and breakdown I-V characteristics for small cylindrical samples of the SDF soil when subjected to voltage pulses. A model is postulated for the breakdown process which involves ionization of the air in the voids between the soil grains, and evidence in support of the model is discussed. A semiempirical equivalent circuit model of the soil/pulser setup during the breakdown is presented and fitted to the measured I-V characteristics. Although the fit to the data is not perfect, the agreement is sufficient to give further credence to the air ionization model. The mathematical formulation of the equivalent circuit model can be used to apply the small-scale breakdown data to more realistic situations of interest.

1. C. E. Mallon, R. Denson, "Low-Field Electrical Characteristics of Soils," Theoretical Notes, Note 315, 12 January 1981.

SECTION II

SAMPLE PREPARATION

The soil samples used in these studies were made from soil collected from the Siege Development Facility (SDF) in Albuquerque. The soil was collected from near the center of the facility as defined by the East and West electrode lines. The appearance of the as-received material was that of very dry soil; however, drying of this material revealed a moisture content of three percent by weight. (Soil with six weight percent moisture has a definite moist appearance.) The material used for sample fabrication was passed through a screen to remove particles with dimensions greater than ~1/16 x 1/16 inch.

The majority of the experiments used the as-received material with a three percent by weight moisture content. For a lesser moisture content, the material weight was monitored while drying until the desired moisture content was achieved. For moisture contents greater than three weight percent, the appropriate weight of distilled water was added. Whenever the moisture content of the as-received material was altered, the altered material was stored for a period of time in a sealed plastic bag to ensure material uniformity.

The parameters that were varied during nonlinear studies were sample length, sample area, and sample moisture. Other parameters such as the soil grain size and compaction, both of which control intraparticle void dimensions, were controlled as follows.

Grain Size. A large quantity of material was strained through a screen at a given time, mixed thoroughly, and stored in a sealed container. Prior to removing material for sample fabrication, the material was again mixed, and the moisture content verified.

Compaction. During sample preparation the required weight of sample material was calculated using a density of 1.5 g/cm^3, the sample area, and the desired sample thickness. This amount of material was then loaded into the sample chamber and compacted by tapping the upper electrode while the sample was subjected to a weight load that approximated the pressure at approximately one meter soil depth. The

sample thickness was then measured and the material density calculated. The sample-to-sample variation in calculated density for this procedure was ~1.5 g/cm^3 ±5%.

The sample electrodes were either solid aluminum or brass with aluminum foil towards the sample. In both cases the aluminum was coated with a thin wipe of Redux* Creme to reduce polarization effects.

The geometry of the sample chamber is discussed in Section 4 of this report.

*Hewlett-Packard Trade Mark

SECTION III

TEST PROCEDURE

For all of the soil breakdown tests, a voltage pulse was applied across the cylindrical samples described in Section II and the voltage across the sample and the current out the base of the sample were recorded on oscilloscopes.

Three different pulsers were used at various times in the program to obtain the increasingly larger voltages required for breakdown as the sample lengths were increased. Two of these pulsers had decay time constants on the order of one microsecond while the time constant for the other was longer than a millisecond. Since each of these pulsers was used for a different set of experiments, it is convenient to describe each pulser at the time the corresponding data is presented in Section IV.

SECTION IV

PRESENTATION OF DATA

A large number of discharges were recorded for three pulser types and only a few representative current (I) and voltage (V) traces will be presented. In general, each of the three pulsers were used in sets of experiments with different specific objectives, which to some extent was dependent on the pulser capability. It was also observed that the initiation of a breakdown and subsequent I versus V behavior was pulser-dependent. For these reasons the following data presentation will be grouped by pulser type and experiment objective.

4.1 SOIL BREAKDOWN EXPERIMENTS WITH THE PULSPAK 10 A (10 kV, 150 ns DECAY) FOR 0.5 cm THICK SAMPLES WITH H_2O CONTENT AS A VARIABLE

These experiments investigated the breakdown threshold and post breakdown I-V characteristics for planar samples with a fixed 0.5 cm length and 20 cm^2 area for water contents between 0 and 6 percent by volume. The time delay to breakdown (t_D) versus electric field was also measured for samples with water content from 2.5 to 6.0 volume percent.

A commercial Pulsar* PULSPAK 10 A pulser was used for this set of experiments. This pulser has a fixed peak output voltage of 10 kV with an RC decay time constant of ~150 ns when operating into a 50 ohm load. (Pulser C ~3 nF, E ~0.15 J). The output of the pulser (Figure 1) was connected to the sample with approximately 370 ft (550 ns) of 50 ohm RG-213 coaxial cable to provide a 1.1 microsecond (≈7 pulser time constants) clear time prior to the return of the wave reflected at the sample. Several techniques were used to vary the voltage at the sample to establish sample breakdown thresholds. For sample voltages of 10 kV or less, a 50-ohm termination at the sample was used in conjunction with fixed series resistive attenuators (10 to 100 ohms) at the pulser output. The series attenuators at the pulser output formed a voltage divider network with the 50-

*Pulsar Associates, Inc., San Diego, California

ohm characteristic impedance of the RG-213 cable. This arrangement provided a voltage range at the sample of ~0.33 to 0.83 times the fixed 10 kV pulser output voltage, for samples whose prebreakdown impedance was large compared to the 50-ohm termination resistor. When voltages greater than 10 kV were required to initiate sample breakdown, the 50-ohm terminator resistor at the sample was removed to provide an increased voltage at the sample due to a positive reflection coefficient. For samples whose prebreakdown impedance was large compared to 50 ohms, this configuration provided a voltage range at the sample from about 7 to 20 kV for series attenuator values of 100 to 0 ohms. (A sample impedance of 500 ohms yields a positive reflective coefficient of +0.9 and results in voltage doubling at the sample.)

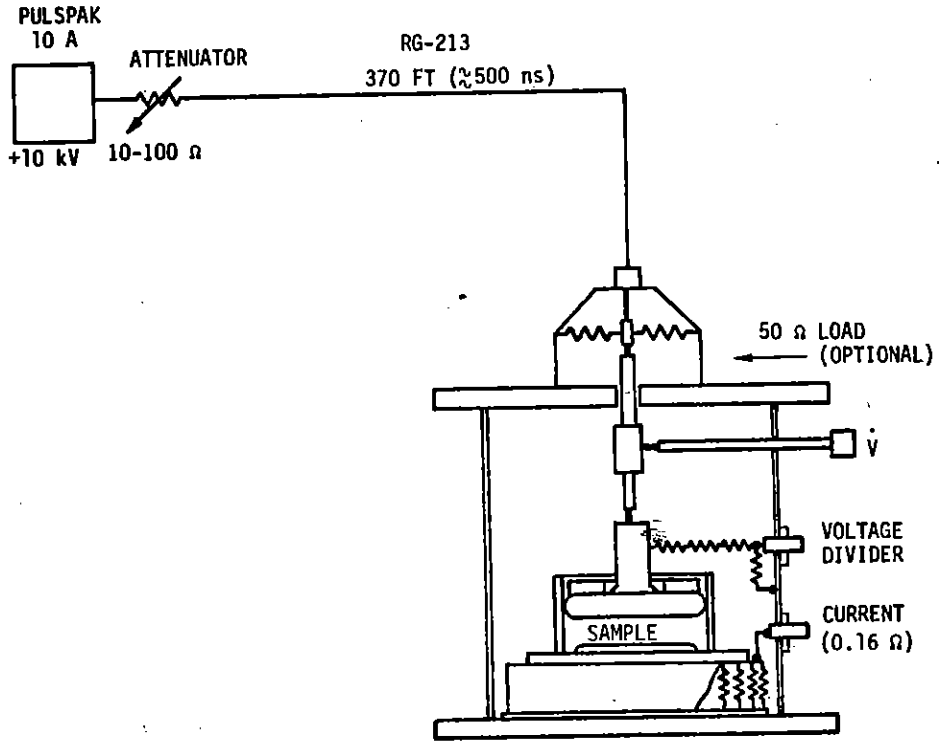

Figure 1. Pulser and circuit used for breakdown experiments with 0.5 cm thick samples

During breakdown experiments the sample voltage was measured by a resistive voltage divider inside the sample chamber (three 3 kΩ resistors in series, with 50 ohms to ground at the output connector) and/or a small metal cylinder placed around the coax cable dielectic/center conductor to form a $C\dot{V}$ probe. Sample current was determined from voltage measurements across a 0.16 ohm current shunt which consists of sixty-two 10-ohm resistors in parallel. To ensure that only current which passes through the sample is measured, the current shunt was placed between the bottom sample electrode and the metal end cap of the cylindrical sample chamber, which returns the sample current coaxially with the sample and current shunt.

The current and voltage sensors were calibrated by substituting known resistive loads for the sample and also by using lower voltage pulsers which allowed a cross-check of the current and voltage sensors with conventional voltage and current probes.

Figure 2 is a drawing of a typical oscilloscope trace during sample breakdown. During the initial voltage rise across the sample, a current spike is observed equal to the product of the sample capacitance and dV/dt ($C\dot{V}$). After the initial voltage rise the current decreases to a value determined by the applied voltage and the sample resistance. For all samples, except the completely dry sample where σ was $\sim 4 \times 10^{-6}$ mho/m, the conduction current during the pulser decay always greatly exceeded the $C\dot{V}$ current. At breakdown, the voltage across the sample decreases rapidly due in part to a negative reflection coefficient that results when the sample resistance decreases to a value less than 50 ohms, and also because of increased voltage drops across other resistive elements in the circuit.

Figure 3 shows examples of oscilloscope traces used to determine the time delay before breakdown and the current and voltage before and after breakdown. These photographs are for a planar SDF soil sample containing 4.5% water by volume. The sample length was 0.5 cm and the electrode area was 25 cm^2 ($\ell/A = 2 \times 10^{-2}$ cm^{-1}). These discharges were produced by the 10 A pulser with a decay time constant of approximately 150 ns. For these discharges, the 50-ohm terminator at the sample chamber (Figure 1) was removed to utilize a positive reflection coefficient and thus create peak voltages greater than 10 kV at the sample. Figures 3(a) through 3(c) illustrate the decreasing time delay to breakdown as the peak applied voltage is increased by decreasing the series attenuator resistance at the output of the 10 A pulser. These photographs each contain 10 pulses. Figure 3(a) shows the variation in time delay when the peak applied field is only slightly greater than the threshold field required for breakdown. Note in Figure 3(a) that for 10

pulses ($E \sim 2.1 \times 10^6$ V/m), 9 discharges are observed while 1 pulse did not produce a discharge. For the 9 discharges, the time delay varied from 135 to 310 ns. Figures 3(b) and 3(c) are for successively larger peak E fields and show a decrease in the time delay to breakdown as well as a decrease in variation of the time to breakdown at larger fields. In Figures 3(b) and 3(c), the sweep speed of 20 ns/div shows clearly the relative magnitudes of the $C\dot{V}$ current during the pulse rise and the subsequent conduction current.

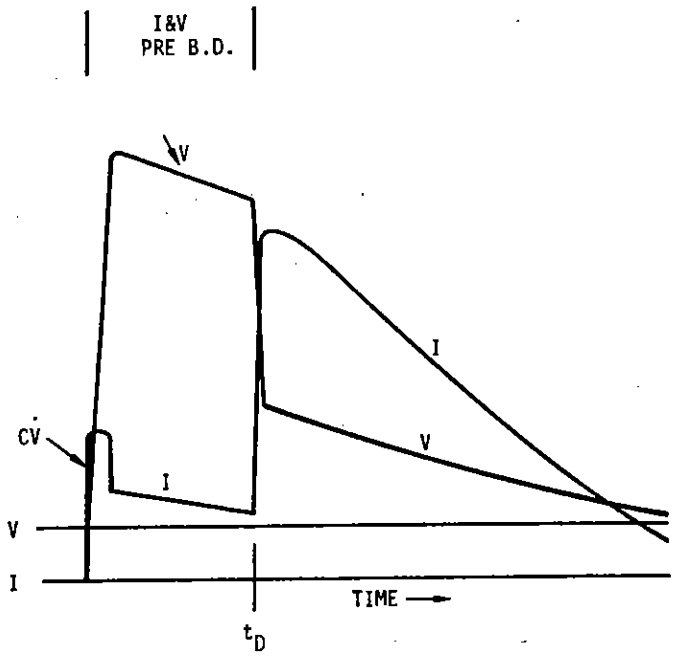

RE-03424

Figure 2. Sample voltage and current before and after a breakdown

Figure 3(d) is an example of oscilloscope traces used to measure current and voltage before and after a discharge where the voltage trace is magnified for greater resolution.

4.1.1 Time Delay to Breakdown Versus Water Content

The time delay to breakdown was measured for 0.5 cm long samples as a function of electric field and water content from 0 to 6 percent by volume. These results are

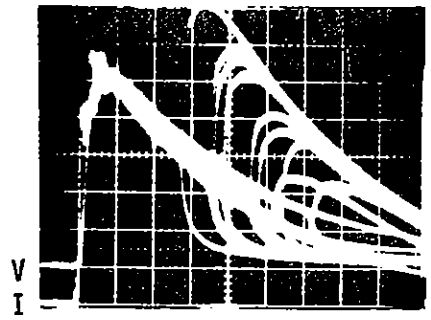

3(a)
V = 2 x 10^3 V/DIV.
I = 16.7 A/DIV.
50 ns/DIV.
SERIES ATTENUATOR = 15 ohms

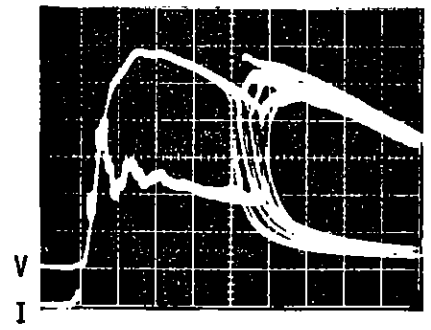

3(b)
V = 2 x 10^3 V/DIV.
I = 33.3 A/DIV.
20 ns/DIV.
SERIES ATTENUATOR = 10 ohms

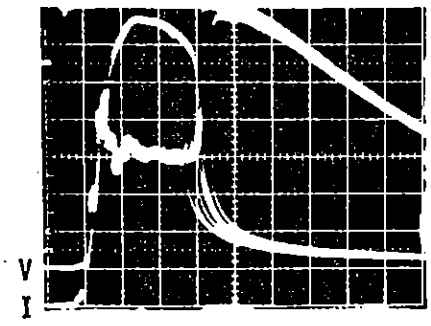

3(c)
V = 2 x 10^3 V/DIV.
I = 33.3 A/DIV.
20 ns/DIV.
SERIES ATTENUATOR = 0 ohms

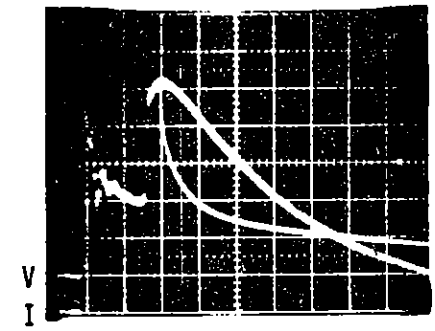

3(d)
V = 508 V/DIV.
I = 33.3 A/DIV.
50 ns/DIV.
SERIES ATTENUATOR = 10 ohms

RE-03526

Figure 3. Example of discharge photographs for a sample with 4.5 percent H_2O (vol.) using 10 A pulser (Figure 1). Sample, $\ell = 0.5$ cm, Area = 25 cm^2

summarized in Figure 4. Near the breakdown threshold field where there is a large variation in the time to breakdown, the data points represent an average for several breakdowns. In Figure 4, time delay is plotted versus the peak applied field. The electric field is calculated using the applied voltage and the electrode spacing. However, as discussed in Section 4.2.2, the electric field may be somewhat larger due to an effective low-impedance contact thickness. The field at breakdown (E_{BD}) can be estimated from

$$E_{BD} \sim E_{PEAK}\, e^{-(t_D/\tau)} , \qquad (1)$$

where t_D is the time delay and τ is approximately 150×10^{-9} s for the 10 A pulser. Only one E field data point was obtained for the completely dry sample as its breakdown threshold was approximately equal to the maximum capability of the 10 A pulser (20 kV with a reflection coefficient of +1). It is interesting to note, however, that near the breakdown threshold the delay time for the dry sample appears to be considerably less than for samples with finite water contents near their breakdown thresholds.

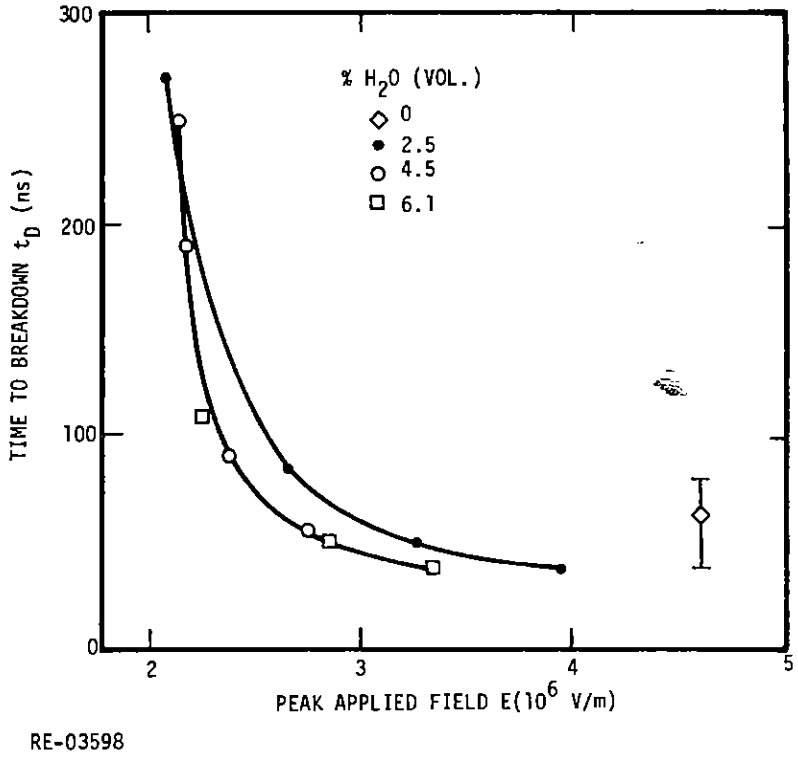

Figure 4. Time delay to breakdown versus peak E field and water content using 10 A pulser. Sample length is 0.5 cm.

4.1.2 Breakdown Threshold Versus Water Content

The effect of moisture content on the breakdown threshold is shown in Figures 5 and 6 for the same samples discussed above. In Figure 5 the peak value of J/E observed after a breakdown is plotted versus the peak applied electric field that produced the breakdown. The observed threshold was well-defined in terms of the peak applied field even though delayed breakdowns would occur at a significantly lower field [see Figure 3(a), where a decrease in the peak applied field of only a few tenths of a MV/m produced no breakdowns]. The breakdown thresholds obtained from Figure 5 are plotted in Figure 6 as a function of water content, and indicates a minimum breakdown threshold for a water content of about 4% by volume, with the largest dependence occurring for a small water content of between 0 and 2.5% (volume).

4.1.3 Postbreakdown Characteristics Versus Water Content for 0.5 cm Samples and the 10 A Pulser

There are various ways to plot the discharge data obtained from photographs such as shown in Figure 3. Prior to breakdown, the electrical conductivity is a well-defined parameter as one can assume that the total area of the sample is involved in the conduction process. After breakdown, a calculated conductivity assumes that the total sample area contributes equally to conduction, which may be incorrect. Therefore, postbreakdown conductivity represents at best an average conductivity. A plot of current versus voltage, however, does not readily reveal the peak conductivity or minimum resistance achieved by the sample during the discharge. (See Figures 7 and 8 which show I versus E and σ versus E for the same breakdown.) Therefore, for these samples we have plotted conductivity versus the instantaneous average electric field and include the necessary geometry factors to obtain the resistance ($R = \ell/A\sigma$), current ($I = \sigma A E$) and voltage ($V = E \cdot \ell$), where A is the sample area, and ℓ is the sample length.

Figures 7 through 11 show examples of reduced breakdown data for a 0.5 cm sample with 2.5% water by volume for increasing applied electric field. Similar plots for samples with different water contents yield the discharge data that was summarized in Figure 5. From the data in Figure 5, the peak conductivity observed after a breakdown does not appear to depend strongly on water content between 2.5% and 6.0% by volume for electric fields about 1 MV/m in excess of the breakdown threshold. Similar data was not obtained

for the dry sample as its breakdown threshold corresponded approximately to the maximum voltage that could be obtained with this pulser configuration.

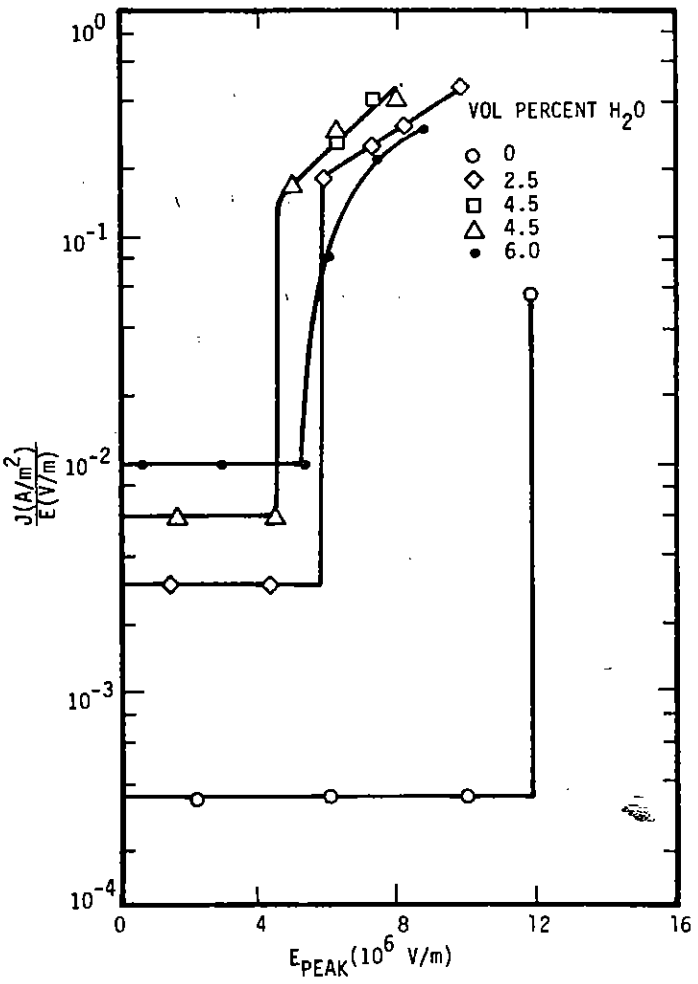

RE-03532

Figure 5. Peak J/E [$(A/m^2)/(V/m)$] versus peak applied electric field for different volume percent water contents. Sample length = 0.5 cm.

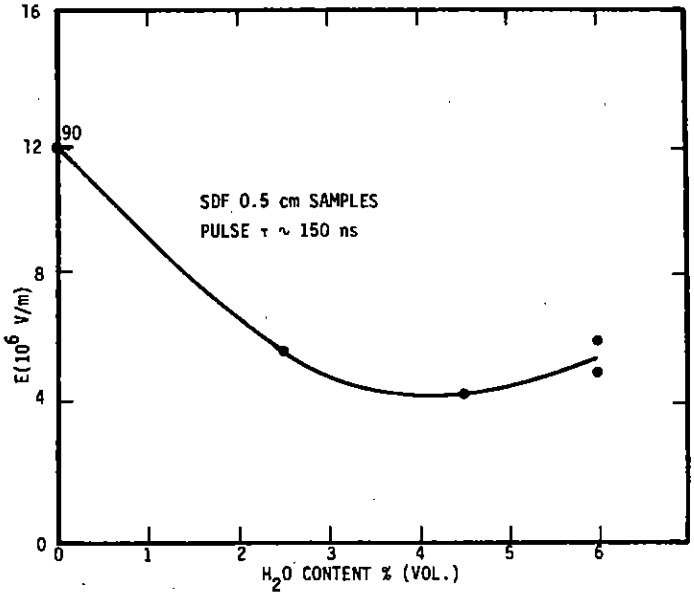

RE-03429

Figure 6. Minimum peak electric field for breakdown versus water content

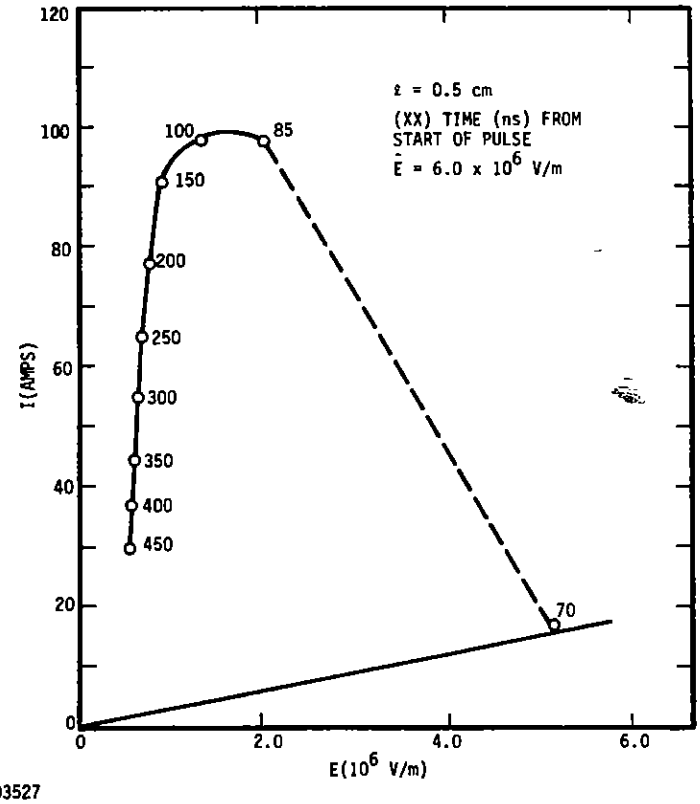

RE-03527

Figure 7. Postbreakdown current versus E field for sample SDF 4 with 2.5% H_2O (vol.) for a peak applied field of 2.2×10^6 V/m. $\ell = 5 \times 10^{-3}$ m, $A = 2.03 \times 10^{-3}$ m^2

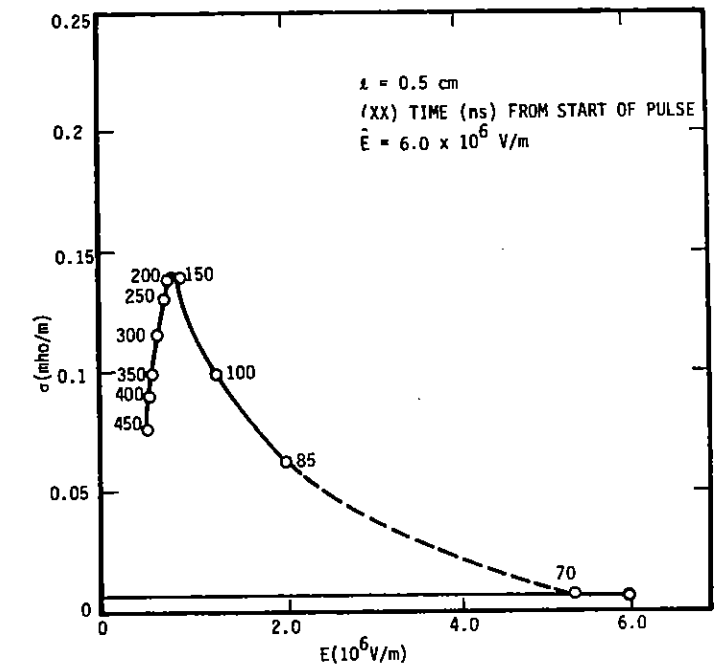

Figure 8. Postbreakdown conductivity versus electric field for breakdown shown in Figure 7.

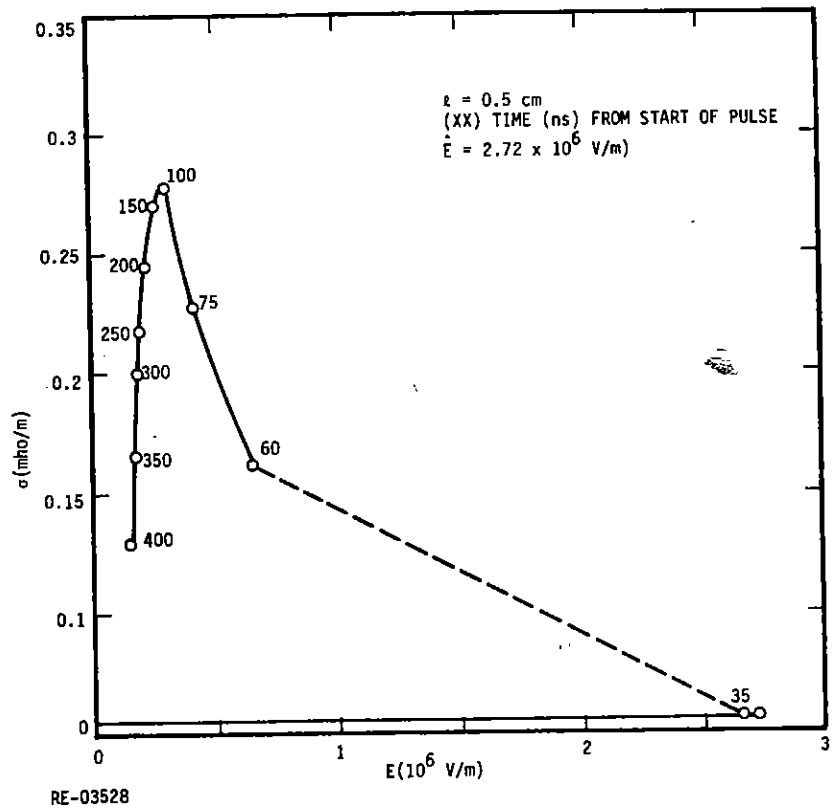

Figure 9. Postbreakdown conductivity versus electric field. Sample SDF 4, 2.5% H_2O (vol.), peak applied field = 2.7 x 10^6 V/m.

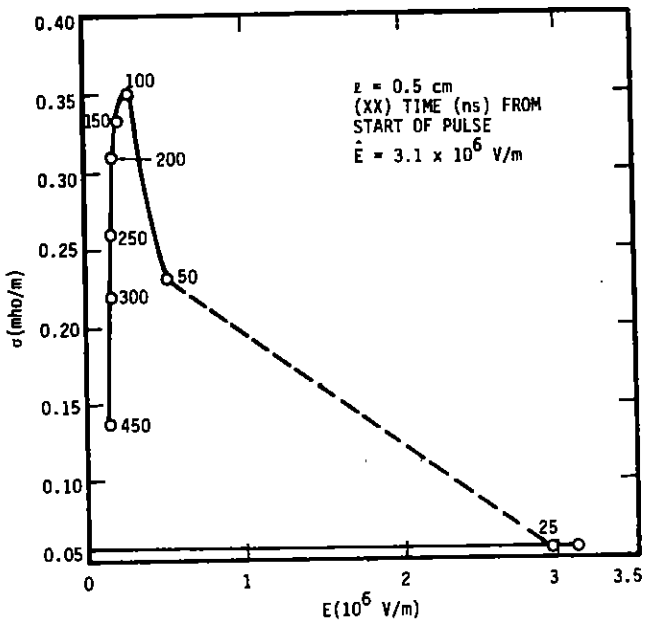

RE-03533

Figure 10. **Postbreakdown conductivity versus electric field. Sample SDF 4, 2.5% H_2O (vol.), peak applied field = 3.1 x 10^6 V/m.**

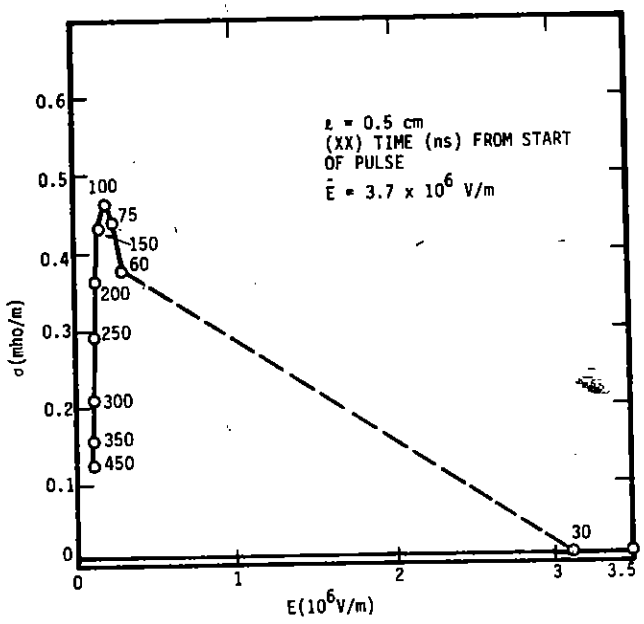

RE-03534

Figure 11. **Postbreakdown conductivity versus electric field. Sample SDF 4, 2.5% H_2O (vol.), peak applied field = 3.7 x 10^6 V/m.**

4.2 BREAKDOWN CHARACTERISTICS IN SDF SOIL VERSUS SAMPLE LENGTH

This set of experiments investigated the breakdown threshold, time delay to breakdown, and the postbreakdown I-V characteristics for samples of various lengths for a constant water content of 4.5% (volume).

In order to produce breakdown in the longer samples (1 to 3 cm), it was necessary to use a pulser that could produce a larger voltage. The circuit for this pulser is illustrated in Figures 12 and 13.

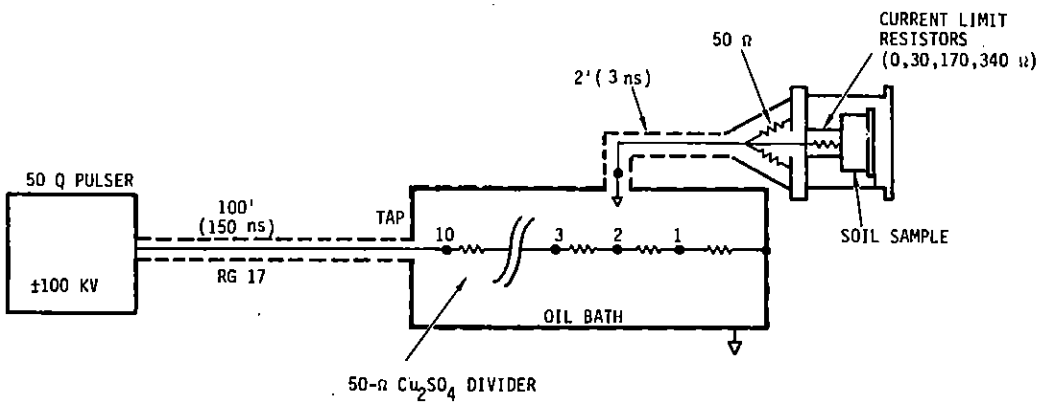

RE-03556

Figure 12. Pulser circuit used for breakdown experiments with 1, 2, and 3 cm samples

The pulser used for samples whose length was greater than 0.5 cm was a PULSPAK 50 Q, manufactured by Pulsar Associates. The 50 Q has a fixed 100 kV peak output voltage with ~17 ns rise time, and about 1.7 microsecond decay time constant into 50 ohms. Unlike the 10 A pulser described previously, the 50 Q must be fired into a near 50-ohm load to prevent damage to the Marx bank by excessive reflected voltages. Since the sample prebreakdown impedance was always >50 ohms, a 50-ohm copper sulfate resistor was made to terminate the 50 Q output cable which was 100 feet (150 ns) of RG-17 coax. In order to vary the sample voltage from the fixed 100 kV pulser output, the

50-ohm copper sulfate termination resistor was segmented with equally spaced taps to provide voltages in 10 kV increments up to 100 kV. A sufficiently long RG-17 cable was not available to provide the desired several microseconds of clear time; therefore, a short length of RG-17 cable whose electrical length was approximately 25% of the pulser rise time was used to connect the sample to the appropriate voltage tap of the copper sulfate resistor (Figure 12). As shown in Figure 13 the sample chamber consisted of a tapered 50-ohm input geometry followed by a 50-ohm termination. The tapered 50-ohm input section was followed by a constant cylindrical section that housed the sample. Plug-in current limiting resistors connected the sample upper electrode to the input of the chamber. The limiting resistors were made up of a combination of series and parallel resistors to minimize inductance and to provide the required current and voltage capability.

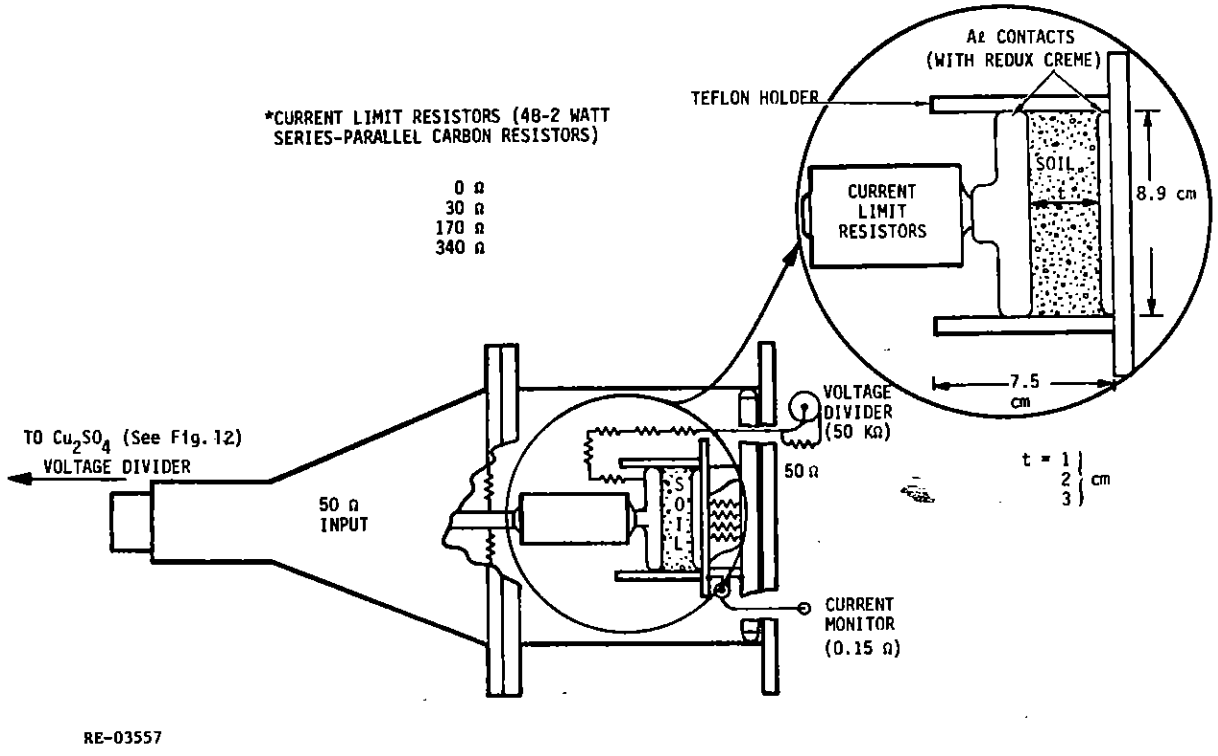

Figure 13. Chamber used for 1, 2, and 3 cm samples during breakdown experiments

Current and voltage measurements were made as described previously, except the voltage divider resistors were increased to five 10^4 ohm-2 W series resistors to accommodate the higher operating voltages.

For a given sample, the experimental procedure was to start pulsing at a tap on the segmented copper-sulfate resistor where the voltage was less than the breakdown threshold, and then increase the voltage in 10 kV increments through the breakdown threshold. This procedure was then repeated for different values of current limiting resistors (0, 30, 170, and 340 ohms) that were inserted between the input cable to the sample chamber and the upper sample electrode (Figure 13). The lower value current limiters were used last as they were likely to result in more severe damage to the sample. At the conclusion of breakdown experiments the sample was always pulsed at lower voltages to determine if the breakdown threshold was decreased as a result of permanent damage. No significant threshold lowering was observed although the samples suffered visible damage. (Postbreakdown photographs are included later in this section.)

Identical soil sample material was used for this set of experiments with sample length being the only variable. The material used was from the SDF site in Albuquerque and is of the same origin as that used for the low-field measurements discussed in Section 1. The water content of the sample was 4.5% (volume), and all samples had an area of 6.24 x 10^{-3} m^2.

Figure 14 shows a typical discharge produced by the 50 Q pulser for a 1.95 cm sample, using Tap 7 (~70 kV) on the copper sulfate resistor and a 170-ohm series resistor in the sample chamber. In the upper photograph the current and voltage gains are such that both prebreakdown and postbreakdown current and voltage traces are on-scale. In the lower photograph, at a slower sweep speed, the voltage trace gain is increased to provide better resolution for the time-dependent voltage determination.

4.2.1 Prebreakdown Characteristics for Samples of 1, 1.95, and 2.89 cm Length

When planar soil samples are subjected to pulses of increasing electric field, a relatively well-defined threshold field to produce a breakdown is observed. Prior to breakdown the sample exhibits an electrical conductivity approximately equal to its low-field value. For example, for the discharge shown in Figure 14 for the 1.95 cm sample, the prebreakdown conductivity is 2 x 10^{-3} mho/m for an electric field of ~2.6 x 10^6 V/m. This

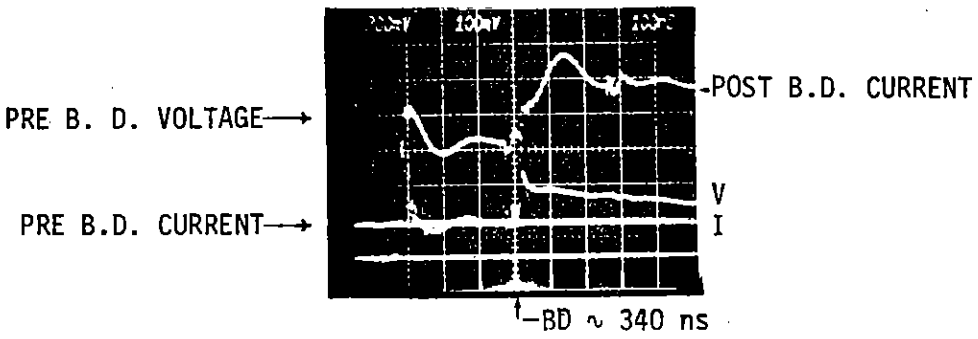

V = 21 KV/DIV.
I = 32.3 A/DIV.
100 ns/DIV.

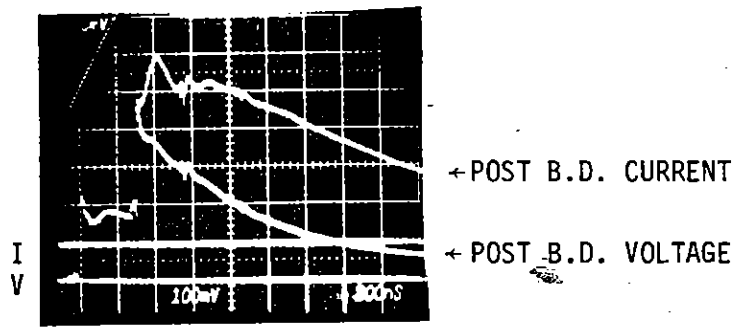

V = 5.3 KV/DIV.
I = 32.3 A/DIV.
200 ns/DIV.

RE-03540

Figure 14. Typical discharge produced by the 50 Q pulser and circuit shown in Figure 12.

value is in close agreement with the low-field LCR measurements for samples with this water content. After breakdown the maximum conductivity, or minimum resistance achieved by the sample is a function of both the applied field and the driver source impedance (i.e., the ability of the source to supply current).

Near the breakdown threshold the time delay, t_D, from the initiation of the pulsed field to breakdown varies considerably. As the field is increased above threshold the time delay decreases and the variation in the time delay for a given field also decreases. Since the voltage across the sample before breakdown is not constant, there is a question as to the most representative voltage to use to characterize the breakdown delay time--for example, the peak voltage, the voltage just before breakdown, or the average voltage over the delay time. We have tried plotting the data as functions of each of these voltages, and the average voltage appears to give the most consistent results. Also, plausibility arguments can be made that it is perhaps the most physically realistic quantity to use.

Figure 15 is a plot of the breakdown delay time for samples with moisture content of 4.5% H_2O by volume versus the average field across the sample for sample lengths of 1.0, 1.95, and 2.89 cm using the 50 Ω pulser. In plotting the points in Figure 15, the effective electrical separation distance between the electrodes for each sample was reduced by 0.36 cm (see Figure 16) because post-test visual examination of the samples indicated that the conducting Redux Creme had penetrated a significant distance into the soil and because it is believed that the threshold field for breakdown, that is, the minimum field at which a breakdown is observed, should be independent of the sample length for these essentially planar samples.

4.2.2 Breakdown Threshold Versus Sample Length

During the experiments to measure breakdown delay time, the minimum electric field (threshold) at the time of breakdown for the three samples was also obtained. In Figure 16 this observed breakdown threshold electric field is plotted versus sample length, where the electric field is that measured at the time of breakdown. In Figure 16 there is an apparent decrease in the breakdown threshold with decreasing sample thickness. Since it is assumed that the important dimension in relating breakdown threshold to the Paschen breakdown voltage versus Torr-cm curve is the void size in the soil sample rather than electrode spacing, one would expect a constant breakdown threshold versus sample length.

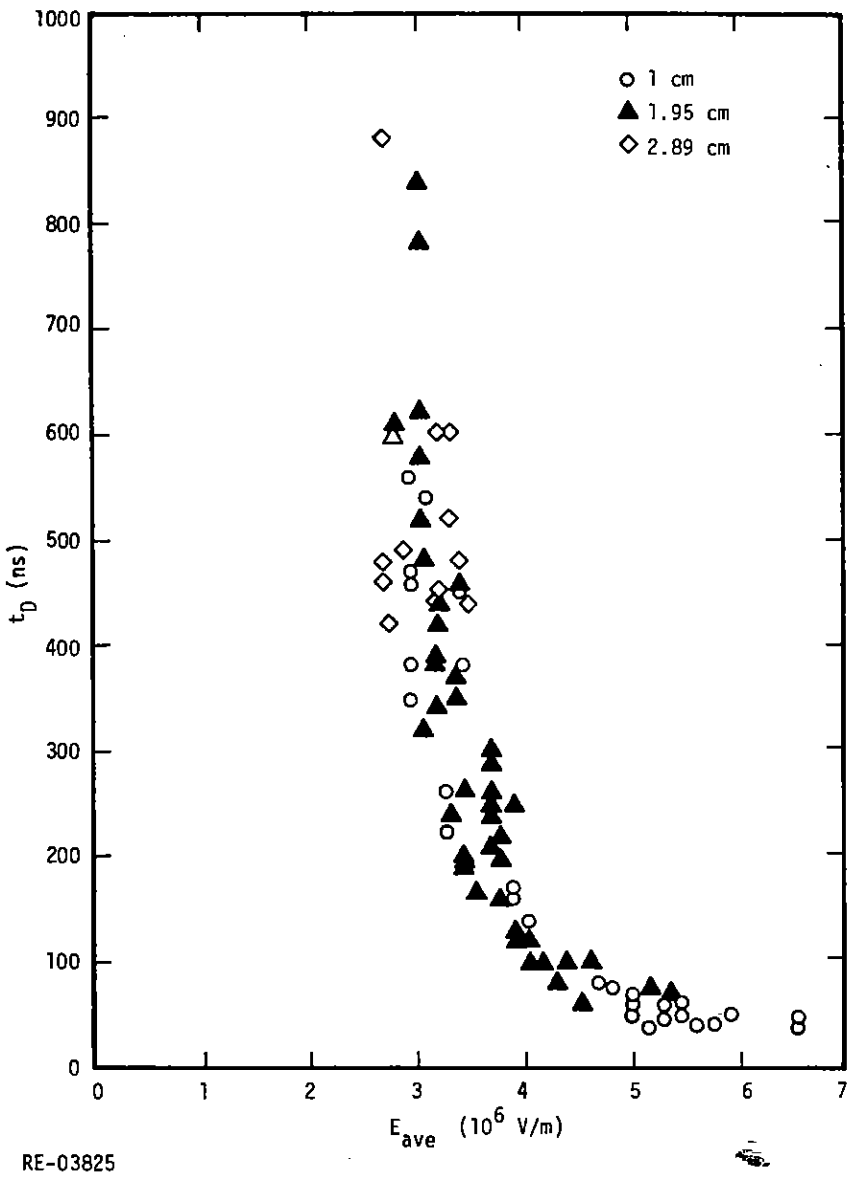

Figure 15. Breakdown delay time versus adjusted average field before breakdown

Postbreakdown inspection of the samples indicate that the method used to contact the samples may have resulted in a finite low-resistance effective contact thickness. As described earlier, a thin wipe of Redux creme was used on the aluminum contacts to minimize polarization effects. When the samples were disassembled after breakdown experiments, the sample surface had a glazed appearance persumably as a result of Redux

interaction with the sample surface, aided by the pressure applied to the electrodes to compact the sample. If an effective low-impedance contact thickness of 0.36 cm (0.18 cm at each electrode) is subtracted from the electrode spacing, the calculated breakdown threshold field shown by the dashed line in Figure 16 is obtained. If the assumption of a finite contact thickness is valid the breakdown threshold for SDF soil samples with 4.5 volume percent water is approximately 2.7 x 10^6 V/m.

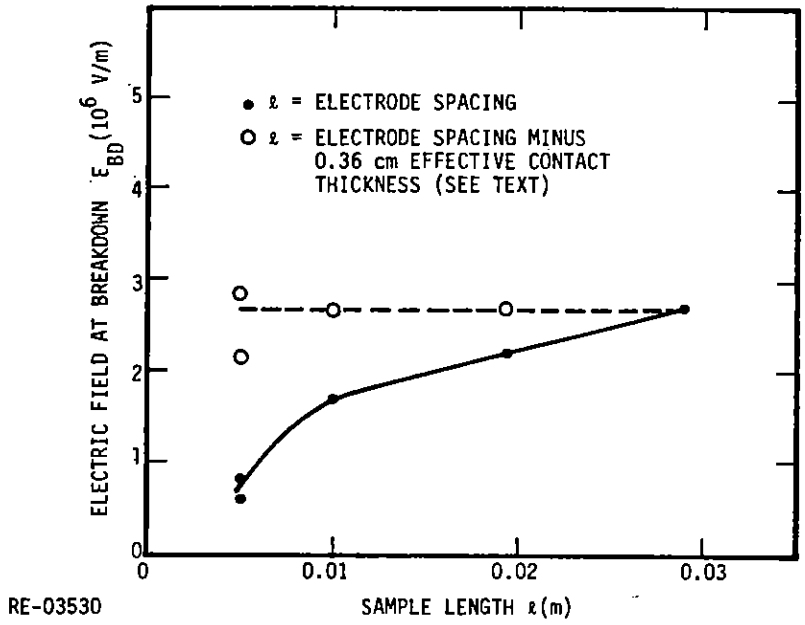

Figure 16. Minimum electric field at which breakdown occurred versus sample length for SDF soil samples with a water content of 4.5% (vol.)

4.2.3 Energy Deposition Prior to Breakdown in SDF Soil Samples with a Water Content of 4.5% (volume)

From the numerous breakdowns produced in the 1, 1.95, and 2.89 cm samples it was possible to extract the average voltage and current before breakdown occurred. Using these average values, and the time to breakdown, the total energy deposited in the sample material prior to breakdown was calculated. These results are shown in Figure 17 where energy (calories) is plotted versus the average electric field before breakdown. The trend is obvious for the 1 and 1.95 cm samples, i.e., as the average electric field increases, the

energy deposited before breakdown decreases. The same trend probably exists for the longer 2.89 cm sample; however, due to the paucity of breakdown data points and the statistical nature of breakdown, this trend is not obvious.

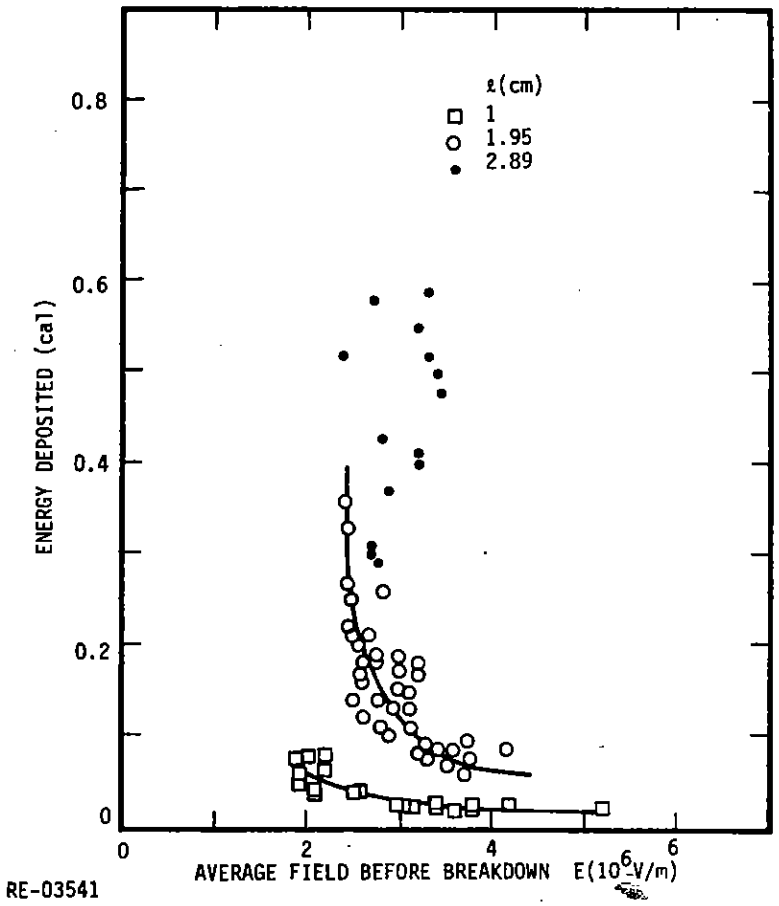

Figure 17. Prebreakdown energy deposition versus the average electric field before breakdown.

The data of Figure 17 allows calculation of an average temperature rise in the sample material before breakdown using the relation

$$Q = mC\Delta T \quad , \tag{2}$$

where Q is the energy input in calories, m is the sample mass (grams), and C the heat capacity (cal/g•°C). Using the maximum energy deposited in the 1.95 cm sample before breakdown of 0.4 calories gives the following temperature rise.

$$\Delta T = \frac{0.4 \text{ cal}}{1.5 \text{ g/cm}^3 \times 1.95 \text{ cm} \times 62.4 \text{ cm}^2 \times 0.2 \text{ cal/g}\cdot^\circ\text{C}} = 1.1 \times 10^{-2\,^\circ}\text{C} \quad . \tag{3}$$

This small temperature rise assumes uniform energy deposition throughout the sample. This assumption appears valid since the measured current and voltage within a few tens of nanoseconds before breakdown yield an electrical conductivity that is in agreement with low-field conductivity data.

The above observations tend to rule out thermally initiated discharges. It is possible, however, for a small fraction of the above energy to be deposited in a small filament and not be detected in the total energy or prebreakdown conductivity. If we assume a deposited energy of 0.1 cal and a temperature rise of 100°C to initiate a breakdown, the filament diameter calculated is ~20 mils for the 1.95 cm sample length. The area ratio of this diameter filament to the total sample area is ~2.7×10^{-5}. Therefore, the conductivity of the filament would have to be several orders of magnitude (~4) greater than the average conductivity to have a measurable affect.

4.2.4 Postbreakdown Characteristics for SDF Soil Samples Versus Sample Length and Pulser Source Impedance

The preceding sections presented data to characterize the initiation of breakdowns. In this section the postbreakdown data for the same samples is presented.

During the design of the experiments using thicker samples and the 100 kV 50 Ω pulser, it was apparent that series protection resistors would be required, especially for the 3 cm sample, where the full output voltage (Tap 10, Figure 12) would be required to produce a breakdown. The sample holder was therefore designed into an existing chamber, shown in Figure 13, which provided the capability of readily inserting different resistance values in series with the sample. The resistance values used ranged from 0 to 340 ohms.

Early in the breakdown experiments it was observed that the maximum conductivity, or minimum resistance of the samples after a breakdown, depended rather strongly on the

source impedance of the pulser circuit. Therefore, a procedure was followed to collect discharge data both as a function of applied electric field and pulser source impedance. In the data presentation that follows the source impedance, R_S, is the sum of the series resistor in the sample chamber and remaining resistance above the tap being used on the 50-ohm copper sulfate termination resistor. Each tap represents a 5-ohm increment; therefore, if Tap 5 is used, 25 ohms remain between the sample connection and the 50 Q output cable.

Figures 18, 19, and 20 show the sample resistance versus the instantaneous voltage after breakdown for the 1.0, 1.95, and 2.89 cm samples, respectively. These figures also include the peak applied electric field, the electric field at breakdown, and the time delay from pulse initiation and onset of breakdown. R_S is the total series resistance between the sample and the output cable of the pulser. All samples show the trend of a decreasing minimum resistance after breakdown with a decreasing pulser source impedance. The data shown in these figures is replotted in terms of an average conductivity versus electric field in Section 5. Section 5 also presents a model for the observed postbreakdown current-voltage characteristics as a function of pulser source impedance.

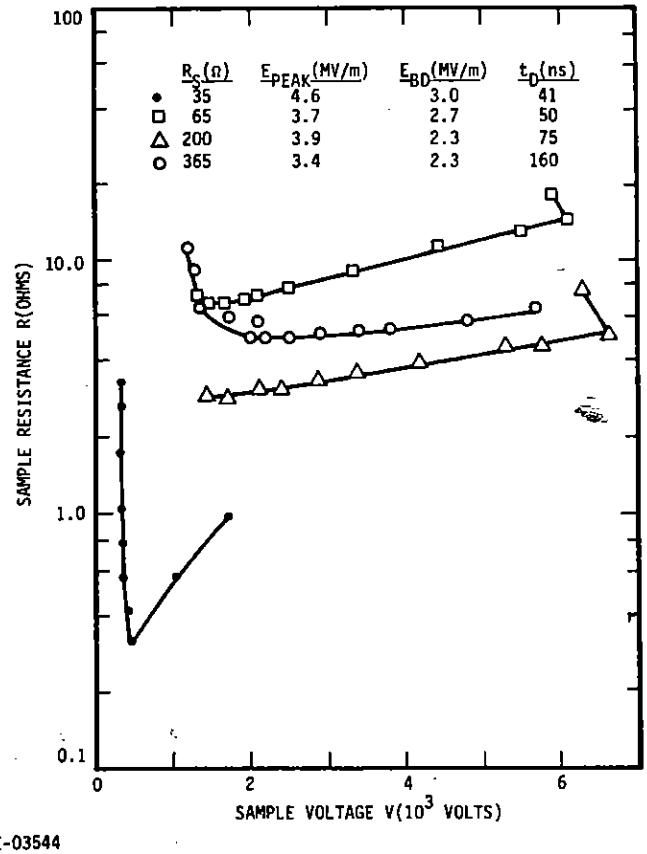

Figure 18. Postbreakdown sample resistance versus voltage and source impedance for the 1.0 cm sample. Area = 62.4 cm^2.

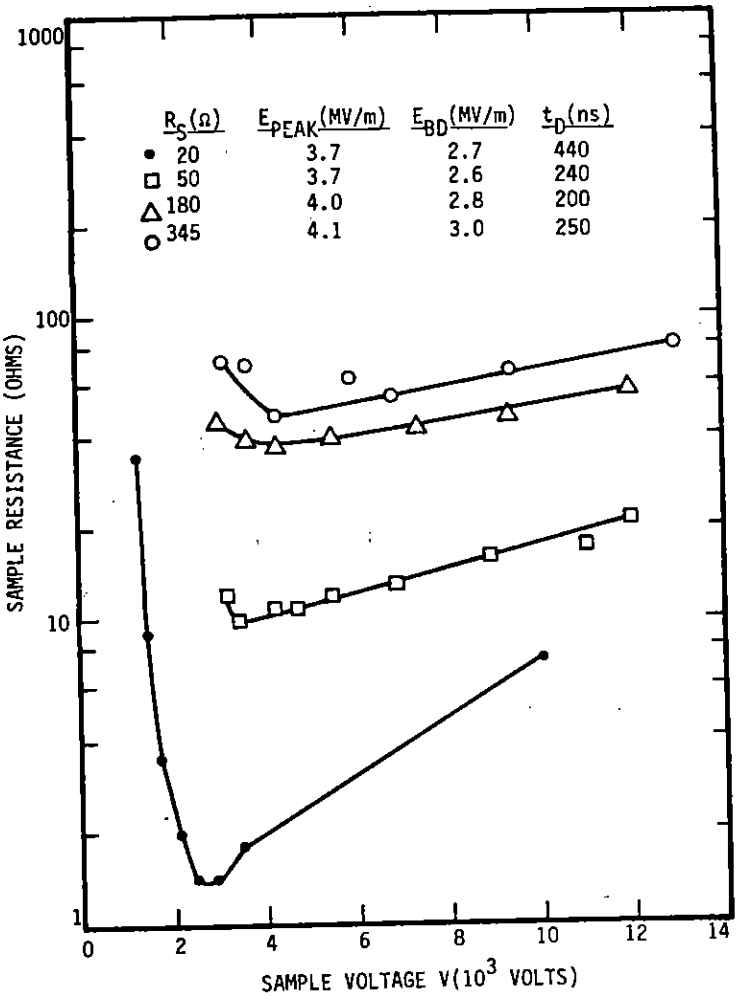

Figure 19. Postbreakdown sample resistance versus voltage and source impedance for the 1.95 cm sample. Area = 62.4 cm^2.

4.2.5 Postbreakdown Examination of Samples and Sample Electrodes

Examination of the sample material and electrodes after breakdown experiments always revealed damage to both the bulk soil and the electrodes. An example of this damage is shown in Figure 21 which is a photograph of the surface of the 1.95 cm sample

after removing the upper electrode. The three major damage areas shown in the photograph (numbered 1, 2, and 3) were voids in the soil that extended the complete thickness of the sample and terminated on the electrodes. The diameter of these voids is approximately 2.5 mm. It was not obvious during the series of breakdown experiments with this sample when these voids formed, and at the conclusion of the experiments the breakdown threshold was not noticeably decreased. A possible reason for the lack of effect of previous breakdown paths on the breakdown threshold is discussed in Section 5.

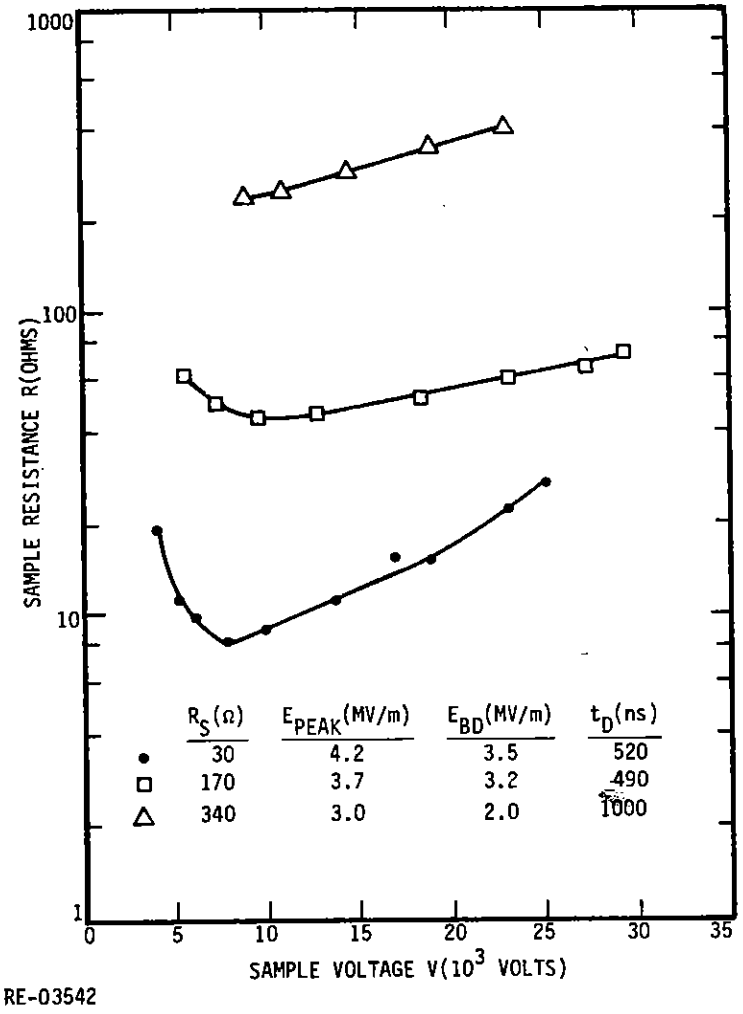

Figure 20. Postbreakdown sample resistance versus voltage and source impedance for the 2.89 cm sample. Area = 62.4 cm^2.

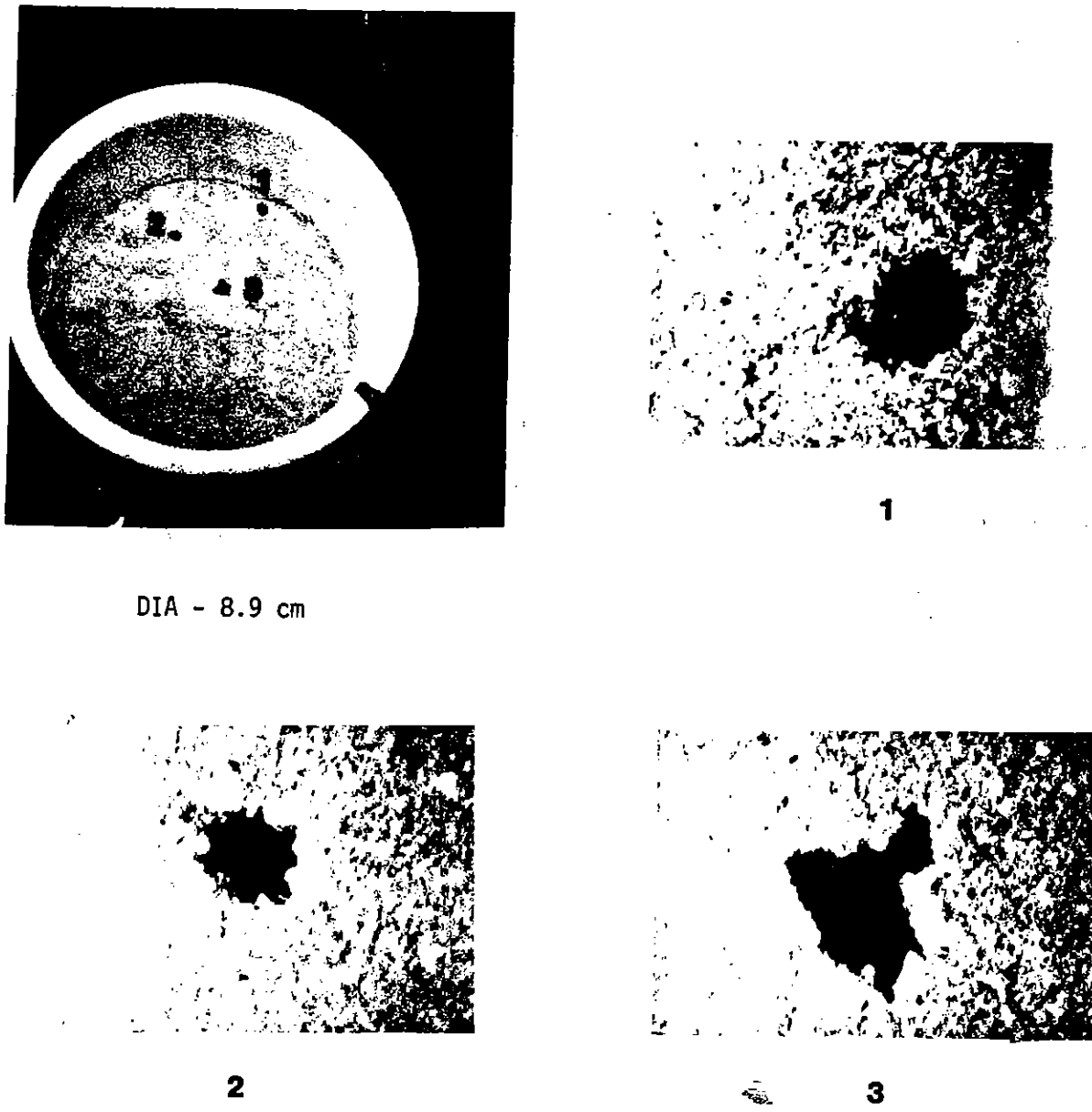

Figure 21. Photograph of damage produced in the 1.95 cm sample during breakdown experiments

Examination of the electrode surfaces revealed numerous small disturbances which did not produce visible damage in the soil material. These disturbances were distributed uniformly over the surface area of the electrodes with a density of $28/cm^2$. Using the total area of the sample electrodes, and the number of breakdowns for this sample, the average number of these small disturbances produced during each breakdown is ~40. These observations are discussed further in Section 5.

4.3 SOIL/DIELECTRIC ROD INTERFACE BREAKDOWN

A brief series of experiments was performed to investigate breakdown in samples with a soil/dielectric rod interface.

The sample chamber used for these experiments is shown in Figure 22. The lower electrode was 5.7 cm diameter and the upper electrode was reduced to a diameter of 2.54 cm. To investigate the effect of a soil/dielectric interface, identical experiments were performed without a dielectric (configuration shown in Figure 22) and with a 0.5 cm long, 1 cm diameter dielectric rod (PVC) inserted between the two electrodes. In both cases, the electrode separation was 0.5 cm. The sample material used had the same origin as that used for experiments discussed earlier in this report and had a water content of 4.5% (volume).

The pulser used for these experiments was designed to stress the sample in the time regime of milliseconds. This pulser was fabricated by JAYCOR and consisted of a 2.18 μF, 12 kV capacitor and a 0-30 kV negative power supply as shown in Figure 23. A 50-ohm resistor pad was used in series with the storage capacitor to damp oscillations. The storage capacitor was manually switched from the charging supply to the sample electrode by a mechanical switch immersed in transformer oil. The pulser rise time was approximately 5 ns.

When used for soil/dielectric interface breakdown studies of planar samples, the impedance of those samples was such that the pulser prebreakdown decay time constant was 10 to 110 ms, where the longer time constant was determined by the 50-kΩ voltage monitor and the storage capacitor.

The results of the experiments indicate a reduced breakdown threshold for the samples with a dielectric rod/soil interface. In this case, a threshold field of 9.5×10^5 V/m was observed, compared with $\sim 1.4 \times 10^6$ V/m for bulk soil in an otherwise identical sample configuration.

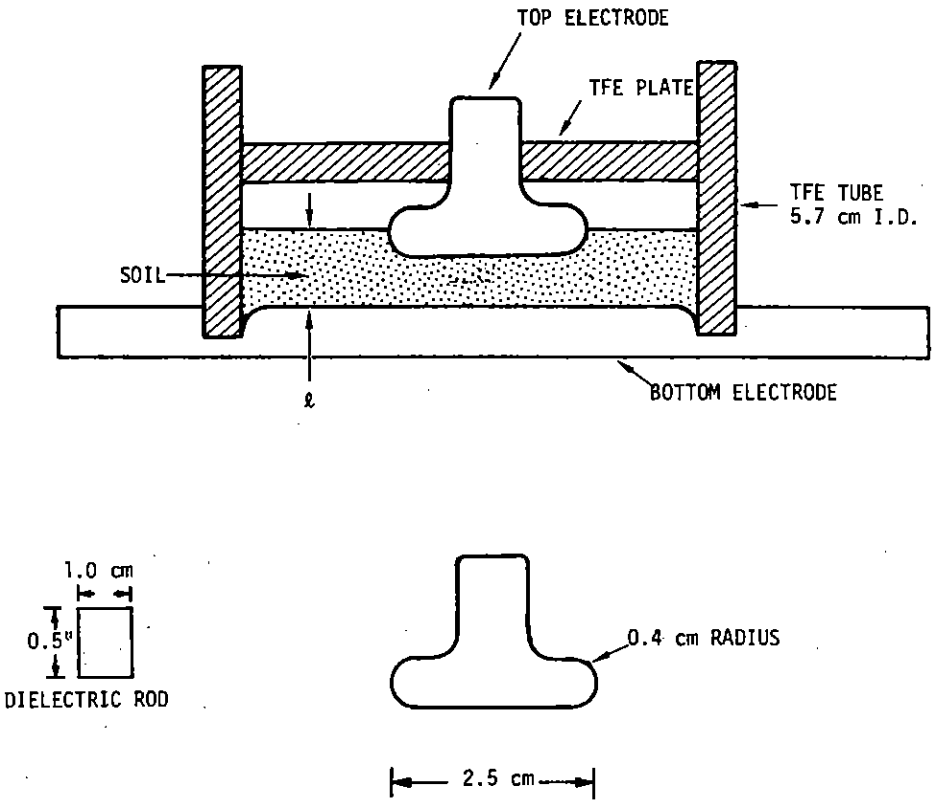

RE-03437

Figure 22. Sample chamber used for soil/dielectric rod interface breakdown experiment.

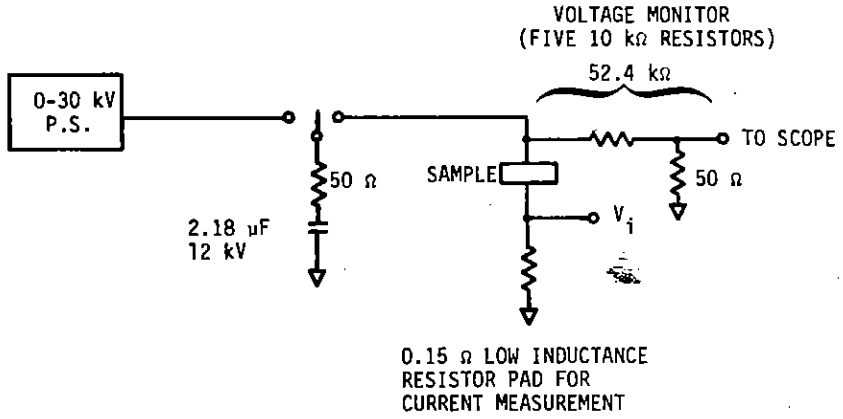

RE-03427

Figure 23. Schematic of pulser used for soil/dielectric rod interface breakdown studies.

Examination of the electrodes and dielectric rod after the breakdown experiment showed evidence that the majority of the breakdowns initiated at the dielectric rod/soil interface. Six pits in the electrode were at or near the rod/soil interface and one was located ~3 mm outside of the interface. Also, the surface of the rod along the discharge paths had an apparent "fire-polished" appearance. Discharges in bulk material without the dielectric rod produced visible electrode pits in a localized region approximately 0.8 cm from the center of the electrode or ~3 mm outside previous rod/soil interface.

From the above observations it appears that the dielectric rod influenced the initiation of breakdowns and also lowered the threshold approximately 40% compared with bulk samples.

4.3.1 Time Delay to Breakdown as a Function of Pulser Decay Time Constant

Section 4.3 discusses the effect of a soil/dielectric interface on the initiation of breakdown in 0.5-cm-thick soil samples. For those experiments, a pulser with a decay time constant of tens of milliseconds was used compared to 150 ns for the 10 A pulser used earlier for breakdown initiation in similar samples. A comparison of the observed time delay to breakdown for the two pulse widths is given in Figure 24. Note that the time delay for breakdown is increased by several orders of magnitude for the 110 millisecond pulse width compared with the time delay observed for the pulser with a 150 ns decay time. At this time, there is not sufficient data to reconcile the large difference in the observed delay times. In Figure 24, the data points for long pulse width represents both the peak applied electric field and the field at breakdown as the pulser decay time constant is much longer than the delay time. The data points for the 150 ns pulser are plotted versus peak applied field. If these data points were plotted versus the average field during the time delay they would shift to the left in Figure 24 and appear more as an extension of the long delay time data points.

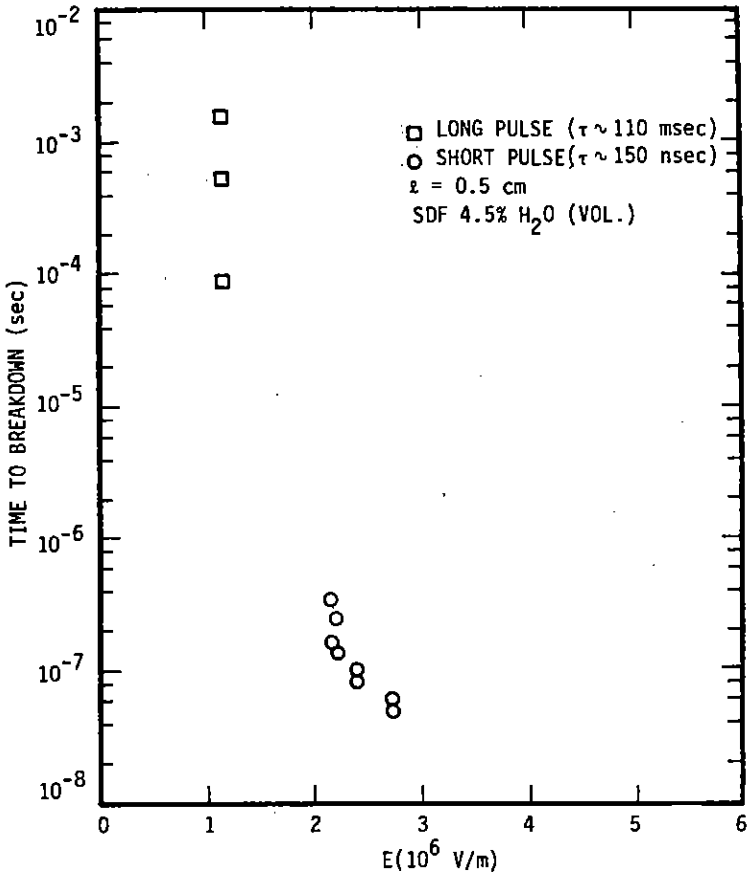

RE-03428

Figure 24. Effect of pulser pulse width on time to breakdown for 0.5 cm planar samples.

SECTION V

PROPOSED MODEL FOR THE BREAKDOWN PROCESS

5.1 GENERAL DISCUSSION

It is generally believed that electrical discharges in dielectrics are triggered at one or more localized spots inside the dielectric and then these breakdown points expand across the dielectric by an avalanche or a streamer-formation process. It is not clear whether these nucleation points occur primarily near the electrodes or are distributed randomly throughout the dielectric. For relatively uniform dielectrics without localized imperfections, the nucleation probably occurs near the negative electrode because a few field-emitted electrons from the cathode are most apt to be in that location to start the avalanche or streamer process.

For soil samples, the situation is more complicated because the dielectric (soil) consists of three different entities, namely, (1) the soil particles themselves, (2) the water content, which presumably coats the exterior of the soil particles, and (3) the air-filled gaps between the soil particles. Thus, there is a question not only how the breakdown is initiated in a soil sample but also which of these three media transport the electrical current that flows before and after a breakdown occurs.

For the discharge model that is proposed here, it is not crucial which medium, or media, carry the current before discharge, which is usually relatively small compared to the peak current during a discharge. However, it is most likely that this current flows through the water layer that surrounds the soil particles since the electrical conductivity of dry soil is quite low and the conductivity of soil is a fairly-sensitive function of its fractional water content.

The following are the central features of the proposed discharge model:

1. The electical breakdown occurs by ionization of the air in the gaps between the soil particles, and the enhanced electrical conductivity of the soil during breakdown is due primarily to charge flow in this ionized air.

2. The threshold field for breakdown is the average field across the sample that produces fields in the soil voids equal to the threshold fields for air breakdown as a function of air pressure and void size.

3. The delay time before breakdown is the sum of a nucleation time for a local avalanche to begin and the time for the local avalanche to propagate across the sample.

4. The I-V characteristics of the sample during breakdown can be modeled as a competition between an avalanche generation rate and an ionization recombination rate, taking into account the voltage and load characteristics of the pulser.

It is not crucial for the present model whether or not the air gaps closest to the electrodes break down first or whether the initial breakdowns occur in the air gaps randomly throughout the bulk of the sample. As stated previously, close to the cathode, there should be a few extra free electrons due to field emission. Since these extra electrons would help to nucleate the breakdown, this fact would favor the initiation of breakdown near the cathode. On the other hand, the voids between the soil particles will usually be quite jagged, which should cause local enhancement of the electric field and thus a higher probability of field emission from the water coating on the soil particles. This critical field could occur at any point throughout the sample. It is quite possible that both types of initiation occur under different circumstances. Which process actually dominates will require further information to resolve. For the present, we just assume that air breakdown does occur in the gaps between the soil particles and compare the resulting discharge characteristics with the corresponding characteristics for simple air gaps.

In this model, the threshold field for breakdown is assumed to be the average applied field (E_a = applied voltage V_a/sample length L) when the field in the air gaps reaches the breakdown threshold for air, taking into account the average relative dielectric constant of the sample ε_r, the field enhancement in the air gaps due to ε_r and the shape of the voids, and the variation of the threshold field for an air breakdown with gap width.

Since there is visual evidence that breakdowns occur along discrete paths, the initial ionization regions apparently expand across the sample from contact to contact in an ionization column, or streamer. This growth of the ionization region is a natural

consequence of the readjustment of the electric fields around a streamer. When ionization begins at a local spot, the electric fields in that region decrease due to the increased electrical conductivity in the ionized region. Therefore, since the voltage across the sample remains essentially constant, the fields in the non-ionized regions have to increase to compensate for the reduced fields in the ionized regions. Thus, the ionized region expands towards the two contacts.

However, as the ionization region expands, there is a competing process of recombination of the ionized species, which tends to quench the streamer formation. In order for a streamer to punch through from one contact to the other, the expansion time of the streamer across the sample must be shorter than the recombination time. Since the expansion rate is undoubtedly a function of the field across the sample, the probability that an initial ionization region will develop into a complete punchthrough should increase with the applied field. Thus, for fields only slightly greater than the threshold fields, a complete breakdown might or might not occur, depending on the duration of the pulse, that is, on the decay rate of the pulser. On the other hand, for larger fields, a breakdown can be expected on every pulse.

The delay time between the initiation of the pulse and the full breakdown is assumed to be the sum of a statistical time for a local ionization to begin plus the time for the streamer to propagate across the sample. Both of these times should be smaller for larger fields. In addition, the propagation time is probably about proportional to the sample length, for the same applied field.

Up until the time that the streamer punches through to both contacts, the current through the sample will be relatively small compared to the current that flows after the breakdown is fully developed. However, once the punchthrough is complete, charge can flow freely between the contacts along the ionization streamer. The equivalent circuit model (Section 5.3) and the experimental data indicate that the average ionization density in the sample continues to grow, at least initially, as the current flows. The magnitude of the soil conductivity, and the resulting current, are limited in the test samples by the quenching (recombination) rate, by the load impedance between the pulser and the sample, and finally by the decay time of the pulser voltage. In situations with an incident EMP wave on the surface of the earth, the current flow and soil conductivity will apparently be governed by the boundary conditions of the illuminated soil region, including the fireball.

From visual examination of various samples after several breakdowns, it is clear that more than one streamer path occurs in the sample. Moreover, several breakdown paths appear to occur on each breakdown. Apparently, a previous breakdown streamer is not a preferred path for a subsequent breakdown because neither the threshold field nor the time to breakdown change significantly with increased number of breakdowns. A possible reason for this effect is discussed later.

5.2 EVIDENCE IN SUPPORT OF MODEL

There are several pieces of information that suggest that this air-ionization model is correct. Unfortunately, none of the evidence is overwhelmingly convincing, but, when it is all taken together, the model is definitely plausible. In addition, none of the available evidence is clearly in disagreement with the model. The different pieces of information are discussed below.

1. In an early breakdown experiment, the sample was immersed in SF_6, which has a breakdown threshold electric field approximately 2-1/2 times larger than the breakdown threshold field for air at the same pressure. For the pulser that was used in that experiment, it was not possible to induce a breakdown with the sample in SF_6 even when the peak voltage was considerably larger than voltages at which discharges were generated when the sample was in air.

2. The threshold breakdown field for atmospheric air versus gap spacing is shown in Figure 25. If one assumes an average width of 5×10^{-3} cm for the soil voids, the breakdown field from Figure 25 should be 1.3×10^7 V/m. By comparison, the measured average field across the soil (E_a = V/L) for breakdown is about 2.7×10^6 V/m, for long samples and when the data for short samples is corrected for possible contact effects (Figure 16). However, the electric field in the voids will be greater than the average field E_a, both due to the relative dielectric constant ϵ_r of the soil and geometry effects. If there were a single spherical void embedded in a dielectric with an unperturbed electric field equal to E_a and a relative dielectric constant ϵ_r, the field in the spherical void would be uniform and equal to (ref. 2)

2. Panofsky, W., and Phillips, W., Classical Electricity and Magnetism, Addison-Wesley Publishing Company, Reading, MA.

$$E_v = \frac{3}{1/\epsilon_r + 2} E_a \quad . \tag{4}$$

At the high frequencies corresponding to nanosecond pulses ($\approx 10^7$ Hz), $\epsilon_r \cong 14$ for soil with modest water content (ref. 1). Therefore, $E_v \cong 1.5\ E_a \cong 4.0 \times 10^6$ V/m. However, there are actually many voids in the soil so the flux lines cannot expand around the voids as is implied by the above formula. In the extreme, if the voids formed a continuous gap across the soil sample, transverse to the electric field E_a, the electric field across this gap would be $E_v = \epsilon_r E_a \cong 3.8 \times 10^7$ V/m. This number could be increased somewhat due to field enhancement at the irregular contours of the voids. The above two estimates of the electric field in the voids (4.0×10^6 V/m and 3.8×10^7 V/m) bracket the breakdown field for an air gap with the estimated width of the soil voids (1.3×10^7 V/m).

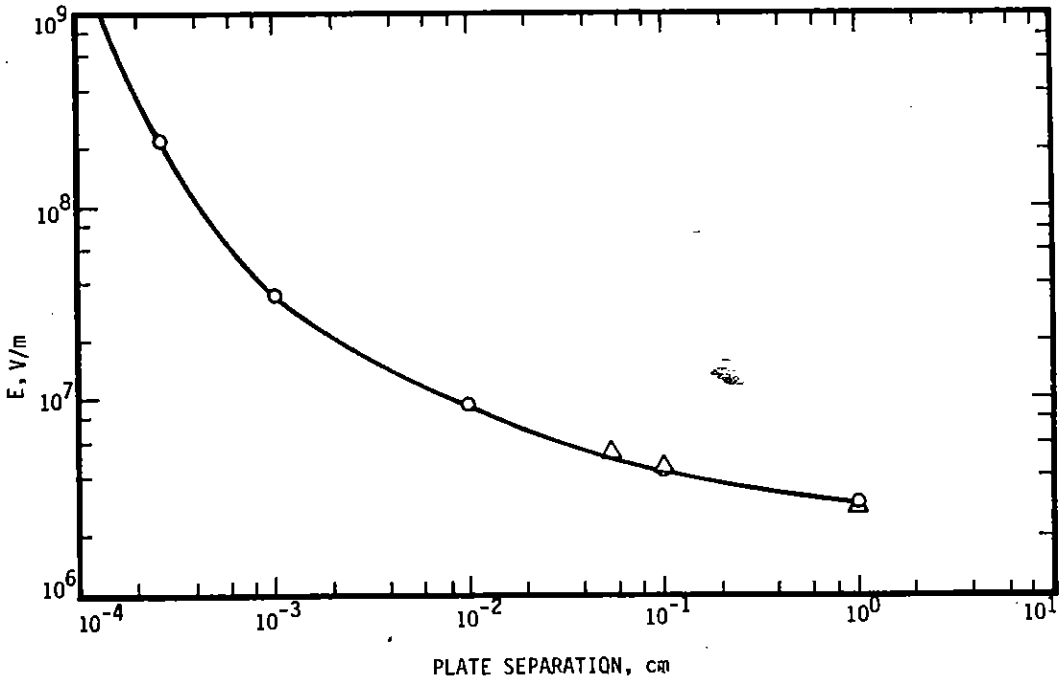

RE-03435

Figure 25. Breakdown field versus separation of parallel plates for air at one atmosphere.

A fairly direct verification of this model could be made by measuring the change in the breakdown threshold field with air pressure and comparing to the Paschen curve for air.

This model is consistent with the fact that a previous ionization path does not appear to be a preferred location for a subsequent breakdown. Suppose that a breakdown burns a hole through the soil from one contact to another, more or less parallel to the electric field. When a subsequent voltage pulse is applied,, the electric field in this long narrow void will essentially be equal to the average electric field E_a across the sample, according to Gauss' law for a narrow void inside a dielectric parallel to the electric field. Thus, the electric field in a previous breakdown path will be less than the electric field in other voids in the soil, so a subsequent breakdown is not likely to be nucleated inside a previous breakdown path.

3. By the Townsend ionization model (ref. 3), the current across a gap becomes unstable (breakdown occurs) when $\gamma e^{\alpha x} = 1$, where γ is the secondary emission yield from the walls of the cavity, α is the avalanche ionization coefficient, and x is the width of the gap. For atmospheric air and $E_{gap} = 10^7$ V/m, α is approximately 3,000/cm (ref. 3). Assuming $\gamma = 0.1$, the breakdown criterion would be satisfied for gaps as small as 7×10^{-4} cm, which is probably smaller than the air gaps between the soil grains. Thus, avalanche ionization in the soil voids at atmospheric pressure appears quite possible at fields on the order of 10^7 V/m.

4. The measured breakdown threshold field for soil with "0%" water is significantly larger than the threshold field for 2-1/2 to 4-1/2% water (Figure 5). At 10 MHz, the relative dielectric constant for the 0% sample was only about 5.5 compared to about 14 for the wetter samples (ref. 1). Thus, based on formula $E_v = \epsilon_r E_a$, the average field E_a has to be about 2.5 times larger for the 0% sample to produce the same (breakdown) electric field E_v across the voids, in rough agreement with the data in Figure 5.

3. Denholm, A.S., et al., "Review of Dielectrics and Switching," Report No. AFWL-TR-72-88, Feb. 1973.

5. The experimental evidence indicates that the "average" electrical conductivity of the sample during the discharge, $\sigma_a = J_s/E_a$, where J_s is the instantaneous average current density through the sample, initially increases with time after the start of the breakdown. Moreover, the equivalent circuit model in Section 5.4 indicates that the rate of increase of σ_a is approximately proportional to J_s. Both of these facts are typical of avalanche ionization processes. However, admittedly, this does not prove that the ionization occurs through the air.

5.3 EQUIVALENT CIRCUIT MODEL

The experimental data indicate that the average current density through the sample ($J_s = I/A$) and the resulting instantaneous average electrical conductivity $\sigma_a = J_s/E$ are fairly sensitive functions of the pulser voltage and load characteristics. Figures 18, 19, and 20 show this dependence on the pulser impedance in terms of the instantaneous resistance of the soil sample for three sample lengths. Since the sample resistance varies with the pulser impedance, an equivalent circuit for modeling the breakdown of the test samples must include the pulser itself. The equivalent circuit that has been used is shown in Figure 26. V_p is the voltage output from the pulser, V_s is the voltage across the sample, C_s is the sample capacitance, R_s is the instantaneous resistance of the sample, R_L is the load impedance, R_1 is the portion of the 50-ohm voltage divider above the divider point, and R_2 is the parallel sum of the portion of the divider resistance below the divider point and the parallel 50 ohms. If we define two electric fields $E_p = V_p/L$ and $E_s = V_s/L$, where L is the sample length, the equation for E_s can be written

$$\frac{dE_s}{dt} = \frac{E_p}{C_s[R_1 + R_L(R_1+R_2)/R_2]} - \frac{E_s}{C_s[R_L + R_1R_2/(R_1+R_2)]} - \frac{\sigma_a E_s}{\varepsilon_s} \qquad (7)$$

where ε is the sample dielectric constant. it will be noted that the equivalent circuit in Figure 27 and Equation 7 do not include effects of inductance in the leads. The consequence of this omission is discussed later.

For purposes of modeling the I-V characteristics of the soil sample, V_p (or E_p) should be a known function of time for each discharge. Unfortunately, V_p was not measured during the discharges. Consequently, curves of the effective V_p during the pulse were calculated using the equation for the equivalent circuit in Figure 26, the known resistances

R_1, R_2, and R_L for each discharge, and the measured curves of I_L and V_s during the discharges. These values of V_p are called "effective" because inductive effects are not included in the circuit model. The values of V_p are essentially the true pulser voltage less the inductive voltages.

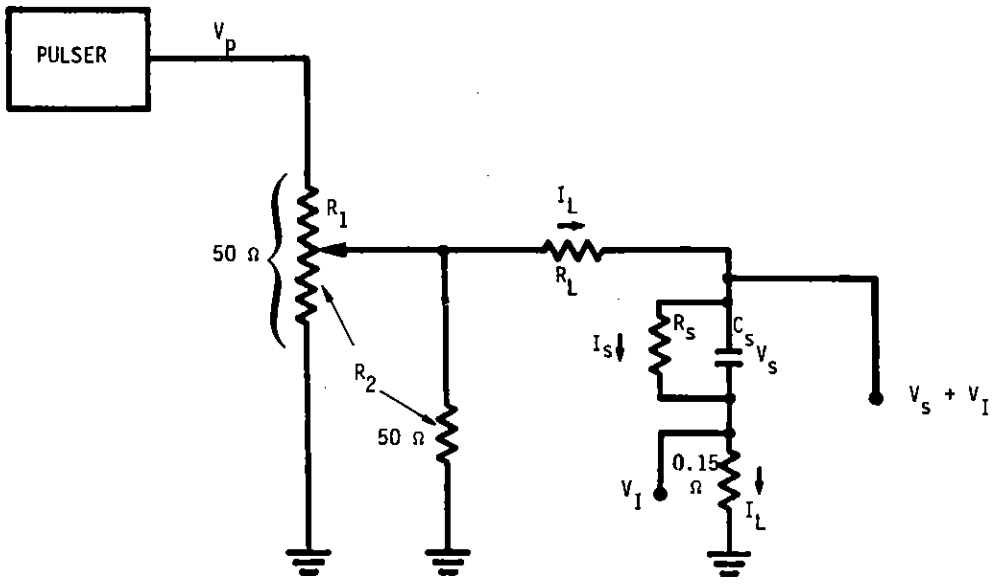

RE-03473

Figure 26. Equivalent circuit for conductivity model

The calculated curves of V_p for the discharges that are analyzed in this report are shown in Figure 27. The data are for two sample lengths (1 cm and 1.95 cm) and four combinations of circuit resistances for each sample length. The solid symbols in Figure 27 at time zero (breakdown) are calculated from the measured values of V_s just before breakdown using the circuit equations and assuming R_s is essentially infinite at that time. It is not clear why these values for V_p just before breakdown do not agree with the extrapolation of the postbreakdown curves back to t = 0. One reason could be the neglect of inductive effects in the circuit model and in the calculated values of V_p after breakdown. If inductance effects could be properly included, the curves of V_p after breakdown would be somewhat different, especially just after breakdown when the current

is changing most rapidly and thus the inductive effects are largest. Unfortunately, measurements of dI/dt from scope traces is rather inaccurate so any attempts to account for inductances would be poor. For the model calculations, the V_p curves were started at the solid symbols at t = 0 and were then joined smoothly into the postbreakdown curves. Uncertainties in exactly how to do this are undoubtedly a factor in the disagreement between the calculated and measured values of σ_a.

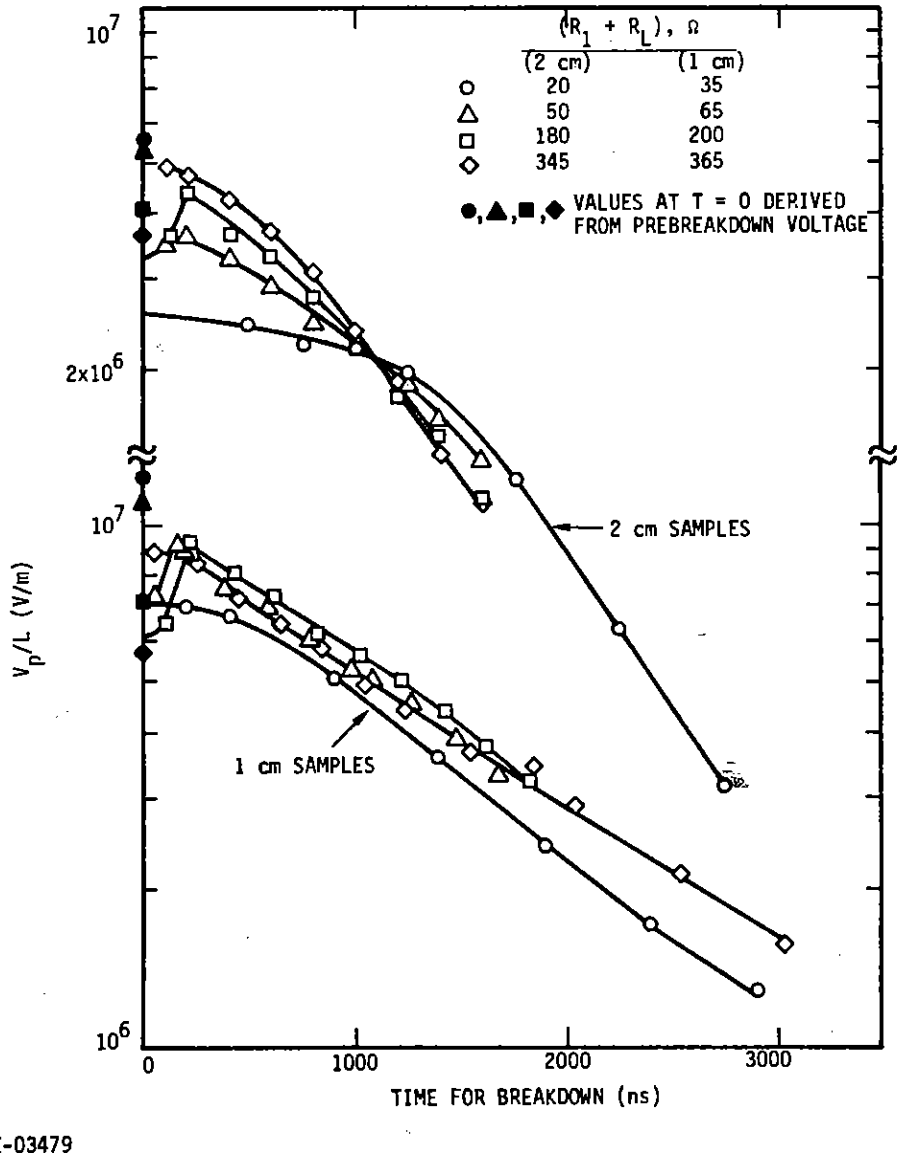

Figure 27. Effective driving voltage for equivalent circuit model

For the relatively fast discharge times of interest (< 1 μ s), ε in Equation 7 can be taken from the low-field data of reference 2 at frequencies around 1 to 10 MHz. Actually, model calculations with different values of ε from 10 to 30 indicated little effect of ε on the time histories of σ_a. Thus, the only unknown in Equation 7, other than the primary variable E_s, is the average conductivity, σ_a.

In keeping with the avalanche model described previously, a differential equation has been assumed for σ_a,

$$\frac{d\sigma_a}{dt} = J_s G_A(E_s, \sigma_a) - \frac{\sigma_a}{\tau_s} = \sigma_a \left(E_s G_A - \frac{1}{\tau_s} \right) \tag{8}$$

where $G_A(E_s,\sigma_a)$ is an ionization generation coefficient, as a function of E_s and σ_a, and τ_s is a characteristic recombination, or quenching, time. If $(E_s G_A - 1/\tau_s)$ in Equation 8 is positive and approximately constant, σ_a will be an exponentially growing quantity with time, like a typical avalanche process. It will continue to grow until E_s becomes small enough so that $E_s G_A$ is less than $1/\tau_s$.

The above model for the soil conductivity has several features which make it similar to the dynamic model for lightening grounding rods in reference 4. The main difference is that the time variation of the resistivity in reference 4 is just assumed, whereas, in the present model, it is a consequence of a differential equation (Eq. 8). For example, in reference 4, the equation for the resistivity ρ, starting from the initiation of breakdown, is written as

$$\rho = \rho_o \, e^{-t/\tau_1} , \tag{9}$$

where ρ_o is the resistivity before breakdown and τ_1 is an adjustable time constant. If we invert Equation 9 to give the conductivity σ in terms of the pre-breakdown conductivity σ_o,

$$\sigma = \sigma_o \, e^{t/\tau_1} . \tag{10}$$

4. Liew, A. C., and Dorveniza, M., "Dynamic Model of Impulse Characteristics of Concentrated Earths," Proc. IEEE, Vol. 121, No. 2, Feb. 1974, p. 123.

This is the same equation as one would obtain from Equation 8 for our model if the quantity ($E_s G^A - 1/\tau_s$) was a positive constant over the time period of interest. Obviously, the difference in the models during this ionization period is that τ_1 is not a constant in the present model. Similarly, in reference 4, the authors write the recovery of ρ to its pre-breakdown value as another exponential ($1 - e^{-t/\tau_2}$), where t is now measured from the start of the decay, times a function of the current density. On the other hand, in our model this recovery occurs when the recombination term in Equation 8 becomes larger than the generation term. The above differences are mainly in the mathematical details, but the basic results from the two models are fairly similar.

A simple computer program was written to integrate the coupled equations, Equation 7 and Equation 8. The initial value of E_s was set equal to the measured value just before the breakdown. The initial value of σ_a was usually taken to be 10^{-3} $(ohm\text{-}m)^{-1}$ but the results were fairly insensitive for values from 10^{-3} to 10^{-5} $(ohms\text{-}m)^{-1}$, except for a slight change in the times at which the electric fields and conductivity occur.

Various functional forms were tried for G_A along with different values for τ_s. A constant value for G_A gave surprisingly good agreement with the experimental data but there were some significant discrepancies. In particular, the calculated curves of σ_a versus E_s for different load resistances tended to be approximately parallel whereas the experimental curves are noticeably steeper for the higher values of σ_a. In addition, the time to reach a given value of E_s became progressively larger for the curves with larger values of σ_a, in contrast to the experimental results.

In an attempt to correct both of these deficiencies in the model, G_A was assumed to have the form $C*F_1(\sigma_a)*F_2(E_s)$, where C is a constant. The empirically selected forms for the dimensionless functions F_1 and F_2 that gave the best fit found to date to the experimental data are shown in Figures 28 and 29, with $C = 5$ $m/V\text{-}s$, and $\tau_s = 8 \times 10^{-7}$ s. It is emphasized that the functions F_1 and F_2 were selected purely to provide the best fit to the data and no attempt has been made to explain the shapes of the curves from physical principles. In fact, it is quite possible that the correct form for G_A is some nonseparable function of E_s and σ_a, and perhaps even a function of the time integral of J_s or $J_s E_s$, that is, of the energy deposited in the sample.

The calculated curves of σ_a versus E_s are compared to the experimental data in Figures 30 and 31 for two sample lengths and four sets of load resistances. These curves of σ_a versus the E_s were derived from Figures 18 and 19 which show sample resistance versus E_s. Time did not permit applying the model to the 2.89 cm sample (Figure 20). Agreement in the magnitude and shape of the curves is quite satisfactory. However, there

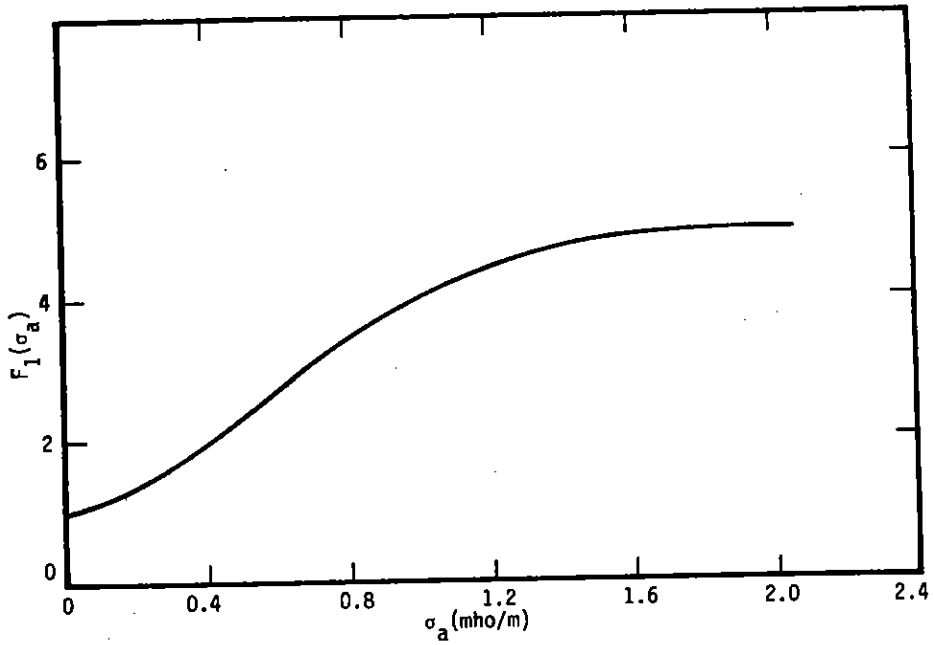

RE-03545

Figure 28. Dimensionless fitting parameter F_1 (σ_a)

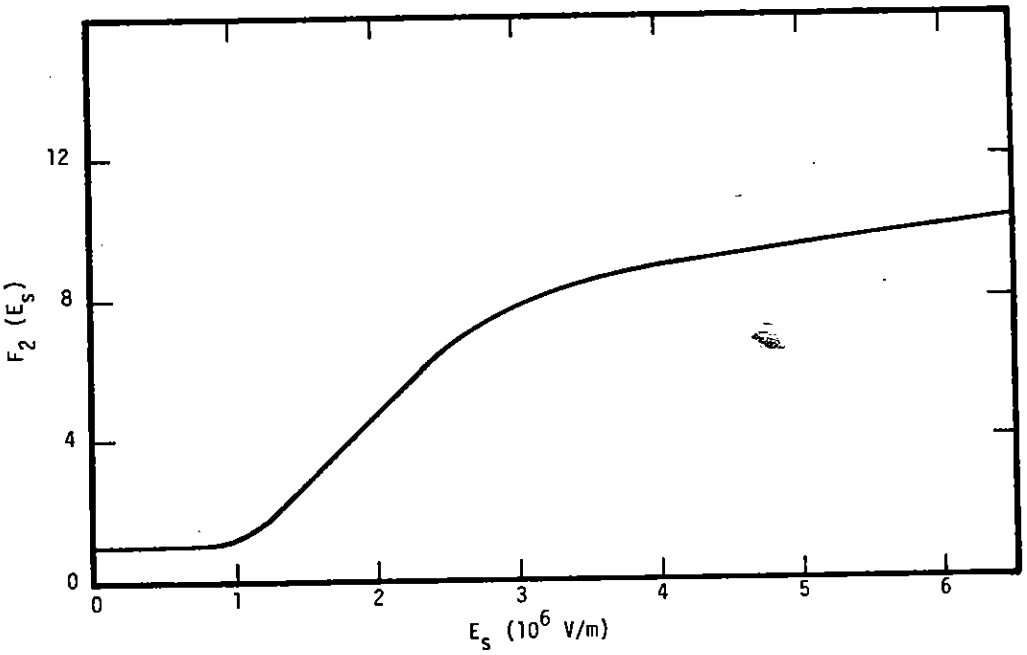

RE-03546

Figure 29. Dimensionless fitting parameter F_2 (E_s)

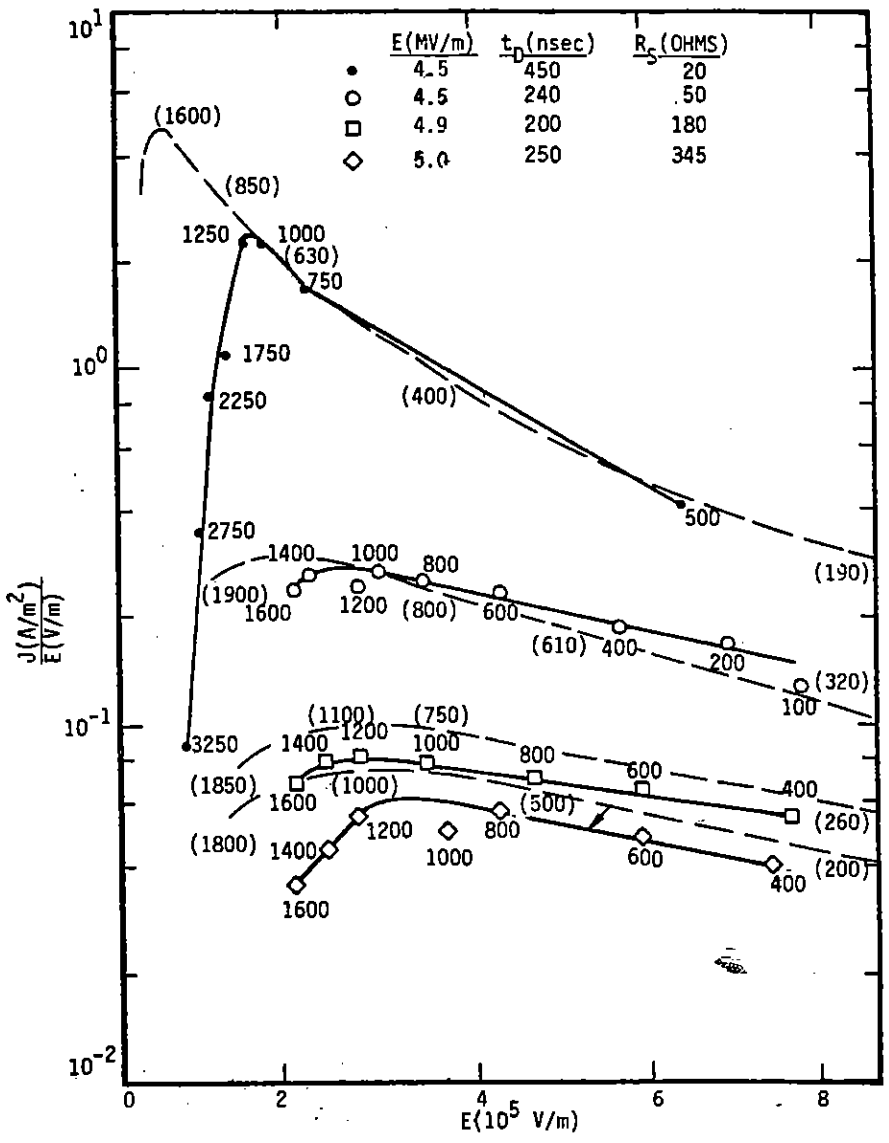

RE-03436(a)

Figure 30. Comparison of experimental and calculated σ_a versus E for different source impedances. Solid curves are experiments. Dashed curves are calculations. Numbers adjacent to curves are times (in ns) from breakdown. Numbers without parentheses are for experiments. Those with parentheses are for calculations. SDF = 4.5% H_2O (vol.), $\ell = 1.95 \times 10^{-2}$ m, $A = 6.24 \times 10^{-3}$ m^2.

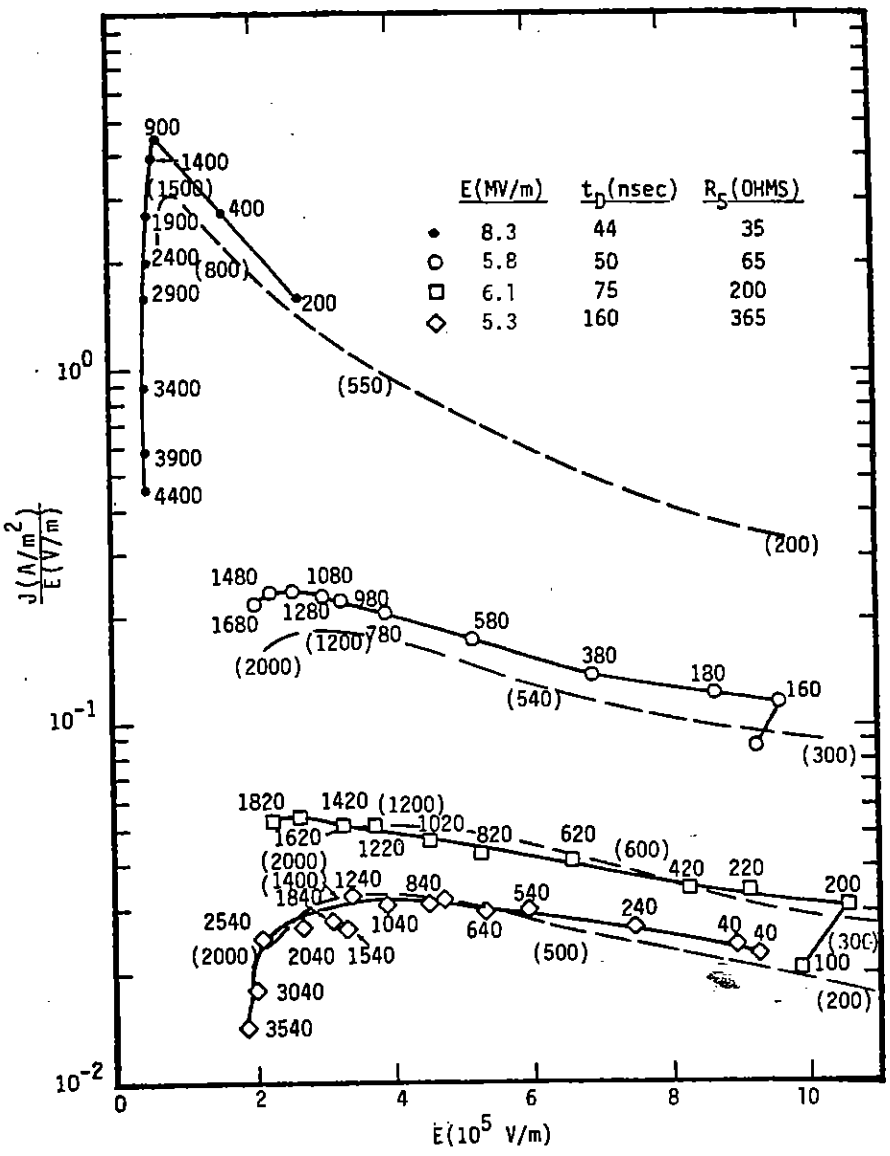

RE-03480(a)

Figure 31. Comparison of experimental and calculated σ_a versus E for different source impedances. Solid curves are experiments. Dashed curves are calculations. Numbers adjacent to curves are times (in ns) from breakdown. Numbers without parentheses are for experiments. Those with parentheses are for calculations. SDF = 4.5% H_2O (vol.), $\ell = 1 \times 10^{-2}$ m, $A = 6.24 \times 10^{-3}$ m^2.

are some noticeable disagreements, especially in the times to reach a given E_s. It is not known if the cause of this disagreement is due to not having chosen the correct functional forms for F_1 and F_2 along with the correct values for C and τ_s, or whether it is due to some defficiency in the model, such as a more complicated function for G_A, or τ_s a function of E_s and/or σ_a, the lack of inductance in the model etc. Another disagreement is the field E_s at which σ_a reaches its maximum at high values of σ_a. This difference might be corrected by a slight change in the curve $F_1(\sigma_a)$ at large σ_a. However, in spite of these disagreements, some useful conclusions can be drawn from the results.

5.4 CONCLUSIONS FROM DATA AND EQUIVALENT CIRCUIT MODEL

The following are the major conclusions that can be drawn from the data and the equivalent-circuit model.

1. The average conductivity σ_a in a soil sample does not have its maximum value immediately after breakdown. Rather, it initially increases with time as a function of the current that is allowed to flow through the sample by the driving source.

2. The rate of change of σ_a appears to be due to an avalanche generation process at early times which competes with a recombination, or quenching, rate at later times.

3. The generation-rate coefficient increases with the magnitude of σ_a, or perhaps with the integral of the energy deposited in the sample.

4. The best-fit model results indicate that the generation-rate coefficient may be quite large at large values of the field across the sample ($E_s \cong 2 \times 10^6$ V/m) and then becomes smaller and nearly constant for fields below 7×10^5 V/m. However, this variation is not conclusively established.

5. For the test samples, the magnitude of σ_a is strongly influenced by the available current from the pulser, as limited by its series resistance to the sample.

6. For modeling the breakdown of soil in a real EMP situation, it is crucial to realistically model the impedances of the source (the fireball) and the final termination of the current path (the conducting shelter and/or ground) so that the current that is available to flow through the soil, and hence the resulting soil conductivity, will be correctly approximated.